AFOSR-TR-88-1181

Second Annual Report

on

Program to Study the
Oxidation of Carbon-Carbon
Composites and Coatings
or These Materials

MATERIALS SCIENCE AND ENGINEERING
University of Pittsburgh
Pittsburgh, Pennsylvania 15261

2

Second Annual Report

on

Program to Study the
Oxidation of Carbon-Carbon
Composites and Coatings
on These Materials

SECURITY CLASSIFICATION OF THIS PAGE

REPORT DOCUMENTATION PAGE

Form Approved OMB No. 0704-0188

1a. REPORT SECURITY CLASSIFICATION: UNCLASSIFIED	1b. RESTRICTIVE MARKINGS
2a. SECURITY CLASSIFICATION AUTHORITY	3. DISTRIBUTION/AVAILABILITY OF REPORT: Approved for public release/ distribution unlimited.
2b. DECLASSIFICATION/DOWNGRADING SCHEDULE	
4. PERFORMING ORGANIZATION REPORT NUMBER(S)	5. MONITORING ORGANIZATION REPORT NUMBER(S): AFOSR-TR- 88-1181
6a. NAME OF PERFORMING ORGANIZATION: Univ of Pittsburgh; 6b. OFFICE SYMBOL (If applicable)	7a. NAME OF MONITORING ORGANIZATION: AFOSR/NE
6c. ADDRESS (City, State, and ZIP Code): Material Science & Eng, Pittsburgh, PA 15261	7b. ADDRESS (City, State, and ZIP Code): Bldg 410, Bolling AFB, DC 20332-6448
8a. NAME OF FUNDING/SPONSORING ORGANIZATION: AFOSR/NE; 8b. OFFICE SYMBOL (If applicable)	9. PROCUREMENT INSTRUMENT IDENTIFICATION NUMBER: AFOSR-86-0251
8c. ADDRESS (City, State, and ZIP Code): Bldg 410, Bolling AFB, DC 20332-6448	10. SOURCE OF FUNDING NUMBERS: PROGRAM ELEMENT NO. 61102F; PROJECT NO. 2306; TASK NO B1; WORK UNIT ACCESSION NO

11. TITLE (Include Security Classification)
Oxidation of Carbon-Carbon Composites and Coatings on These Materials

12. PERSONAL AUTHOR(S)
Pettit, Meier, Schaeffer, Gulbransen

13a. TYPE OF REPORT	13b. TIME COVERED	14. DATE OF REPORT (Year, Month, Day)	15. PAGE COUNT
Annual Report	FROM 15 Jul 87 TO 14 Jul 88		

16. SUPPLEMENTARY NOTATION

17. COSATI CODES			18. SUBJECT TERMS (Continue on reverse if necessary and identify by block number)
FIELD	GROUP	SUB-GROUP	

19. ABSTRACT (Continue on reverse if necessary and identify by block number)

Carbon-carbon composites are being considered for aerospace applications due to their light weight and excellent mechanical properties. Depending upon the application, carbon-carbon composites are expected to be used for periods ranging from about 10 hours to a few thousand hours at temperatures above 1000°C and approaching 2200°C. A major problem in using such materials in oxidizing environments is that carbon reacts with oxygen forming gaseous carbon oxides. Two approaches are being examined to protect carbon-carbon composites in oxidizing environments, in particular, the use of inhibitors to slow down the reactions, and the use of coatings whereby a barrier is developed between the composite and gases which limits the reaction rate.

20. DISTRIBUTION/AVAILABILITY OF ABSTRACT	21. ABSTRACT SECURITY CLASSIFICATION
☐ UNCLASSIFIED/UNLIMITED ☐ SAME AS RPT. ☐ DTIC USERS	UNCLASSIFIED

22a. NAME OF RESPONSIBLE INDIVIDUAL	22b. TELEPHONE (Include Area Code)	22c. OFFICE SYMBOL
SCHIOLER	(202) 767-4933	NE

DD Form 1473, JUN 86 — Previous editions are obsolete. — SECURITY CLASSIFICATION OF THIS PAGE

Second Annual Report
on
Program to Study the
Oxidation of Carbon-Carbon Composites
and Coatings on these Materials

by

J. Cullinan, J. Schaeffer, E. A. Gulbransen
G. H. Meier and F. S. Pettit

Materials Science and Engineering Department
University of Pittsburgh
Pittsburgh, PA 15261

for

Grant No. AFOSR-86-0251
Air Force Office of Scientific Research
Bolling Air Force Base, DC20332-6448

August 31, 1988

Period Covered July 15, 1987 - July 15, 1988

INTRODUCTION

Carbon-carbon composites are being considered for aerospace applications due to their light weight and excellent mechanical properties. Depending upon the application[1], carbon-carbon composites are expected to be used for periods ranging from about 10 hours to a few thousand hours at temperatures above 1000°C and approaching 2200°C. A major problem in using such materials in oxidizing environments is that carbon reacts with oxygen forming gaseous carbon oxides. Two approaches are being examined to protect carbon-carbon composites in oxidizing environments, in particular, the use of inhibitors to slow down the reaction rates, and the use of coatings whereby a barrier is developed between the composite and gases which limits the reaction rate. It has been proposed that boron and phosphorus additives which form B_2O_3 and P_2O_5, can inhibit the oxidation of carbon [2]. Furthermore, a number of protective coatings are being considered to prevent oxygen from reacting with carbon [3,4]. These coatings rely on the development of oxide films which provide protection by inhibiting oxygen diffusion. A typical coating under consideration is chemical vapor deposited (CVD) silicon carbide which forms a silica film during oxidation that acts as a diffusion barrier. A problem arises in attempting to use coatings to protect carbon-carbon, since thermal expansion coefficient mismatch between the composite and the coatings causes the coating to crack. Frequently, composite systems contain additives which upon oxidation form liquids that can seal such cracks [3]. Luthra [1] has compared the oxidation rates of some uninhibited carbon-carbon composites to calculated rates based upon gas phase diffusion and a surface reaction as rate-limiting steps (Figure 1). This comparison shows that the oxidation of carbon is limited by gas phase diffusion at temperatures above about 600°C, whereas a surface reaction controls the rate at lower temperatures. Selected data from the current program and acceptable rates of oxidation of carbon-carbon for short- and long-term applications are also included in this figure. The actual rates of oxidation are orders of magnitude greater than the acceptable rates at temperatures above 600°C. If carbon-carbon

composites are to be used at temperatures above 600°C in oxidizing environments coatings must be used. Figure 1 indicates that Al_2O_3 coatings on graphite can reduce the ablation rate by two orders of magnitude at 1000°C[5]. Moreover, in view of the sensitivity of coatings to cracking, the inhibition of the oxidation reaction must be examined, and utilized as effectively as possible.

Another problem encountered in using carbon-carbon composites arises due to variability in fabricating these materials. For example, the SiC conversion layers often penetrate deeper through the matrix than through the fibers[6]. The nonuniformity in conversion layers and other aspects of the composites occur, in part, because carbon-carbon composites have not been well characterized. This arises for at least two, and perhaps three reasons. First, the processes used to fabricate carbon-carbon composites are proprietary, therefore, there is some reluctance by the companies owning these right to describe the characteristics of their materials. Second, the technical personnel associated with the development of carbon-carbon have not had expertise in the detailed characterization of materials. It, therefore, appears that all the techniques available for characterization of materials may not have been used. Finally, carbon-carbon is a material whose microstructure may not be easily characterized. It is composed of fibers in a porous matrix and great care must be used with conventional metallographic techniques to prevent pulling out portions of the less tough matrix. As a result of these conditions, very little is known about carbon-carbon. It is necessary to develop a methodology to evaluate it. An initial step in developing this methodology is detailed characterization of the as-processed materials.

The objectives of this program are directed at the technical deficiencies which currently exist in carbon-carbon composites. The oxidation of carbon-carbon composites, inhibited composites, and coated composites is being studied. In these studies state-of-the-art materials are being used. Prior to the oxidation studies, the carbon-carbon specimens are being thoroughly characterized using metallographic techniques that have been used previously for

the characterization of metallic systems. The oxidation studies are directed towards describing mechanistically the various rate-determining steps as a function of temperature, gas composition, and fabrication condition. In the latter part of this program, after the oxidation of the state-of-the-art systems have been studied and understood, some new concepts are to be examined in regard to utilizing and optimizing inhibition effects, and to explore new coatings approaches.

This program consists of four phases. The first phase involved the procurement and characterization of the materials to be used in the oxidation studies. The second phase is concerned with oxidation studies using uncoated carbon-carbon (both inhibited and uninhibited)and the effects of water vapor on their oxidation behavior. The third phase involves oxidation studies of the coated materials. The fourth phase will involve the studies to examine new approaches to obtain more resistant carbon-carbon composite systems, and will utilize results generated in Phases I, II and III.

WORK PERFORMED DURING THE SECOND YEAR OF THE PROGRAM

During the current report period, work has been performed on Phases I, II and III of this program. In particular, materials have been obtained and characterizaton studies have been initiated. Equipment to perform the oxidation studies has been constructed and oxidation studies have been performed under a wide range of conditions.

Procurement of Materials

In order to select materials for this program, a variety of carbon-carbon materials have been obtained from HITCO (1600 West 135th St., Gardena, CA). These are:

HITCO #139E Uninhibited Carbon-Carbon.

HITCO #139C Uninhibited Carbon-Carbon with extra heat treatment.

HITCO #136E Inhibited with elemental B.

HITCO #137E Inhibited with B_4C.

Coated C-C #137 plus SiC pack cementation coating.

Characterization of Carbon-Carbon Composites

The composites under study were fabricated from weaves of graphite fibers which were consolidated into a green body by painting with pitch or phenolic and curing to produce fibers in a porous matrix. The green composites were vacuum-pressure impregnated with pitch or phenolic, which was pyrolized to produce a more dense carbon matrix, and final densification was performed by chemical vapor deposition of carbon from methane gas. Inhibited composites were prepared by impregnation with either elemental boron or B_4C prior to the vacuum-pressure impregnation. The exact details of the fabrication procedure are proprietary and have not been communicated by HITCO.

The as-processed microstructure of CC 139E(uninhibited) composite is shown in Figure 2. The top micrograph shows the CVD carbon coating. The fissures are the result of unequal thermal contraction between the coating and composite. The CVD coating has apparently only densified the near-surface regions of the composite. The middle and bottom micrographs show the through-thickness and planar sections, respectively, of the composite.

Figure 3 shows the structure of CC 136E(boron inhibited) composite. The upper micrograph shows the CVD carbon layer which penetrates only a short distance into the composite. The lower micrograph shows relatively coarse B_4C particles among the fibers. Figure 4 is a SEM micrograph and boron x-ray map of one of these particles. The B_4C particles have apparently formed by reaction between the inhibitor and matrix carbon.

Figure 5 shows the structure of CC 137E(B_4C-inhibited) composite. The upper micrograph shows the CVD carbon surface layer and the middle and bottom micrographs show the through-thickness and planar sections, respectively. The B_4C particles cannot be easily resolved in the SEM micrographs but they have been observed by optical microscopy and their crystal structure confirmed by x-ray diffraction. The particles added to CC 137E are roughly one order-of-magnitude smaller than those formed by reaction in CC 136E. The upper micrograph in Figure 6 is a TEM micrograph of a region of CC 137E showing both fiber and matrix. The SAD pattern at right shows continuous graphite rings indicating the presence of a microcrystalline phase. Superposed on the ring pattern are intensity maxima in the 004 ring which are aligned normal to the fiber axis.(Intense maxima also exist in the 002 ring but are obscured by the bright halo in the center of the pattern.) The lower micrograph is a dark-field micrograph using one of the 002 maxima and indicating a preferred orientation of the crystals in the fiber while the crystalline regions of the matrix are seemingly randomly oriented. Figure 7 is a higher magnification micrograph of the matrix showing what have tentatively been identified as microcrystalline regions in a glassy matrix. A conclusive determination of this structure is difficult since the distribution of the regions is too fine to allow the selected area aperature to be centered over only one region.

Oxidation Studies

Specimens of uninhibited and inhibited carbon-carbon composites have been oxidized in flowing oxygen at temperatures between 500 and 1300°C and flow rates between

14 and 550 cm^3/min. The above flow rates correspond to linear velocities between 0.03 and 1.16 cm/sec. Two specimen sizes have been standardized for the tests: Large Size(25x10x4 mm, Bulk Surface Area≈ 7.8cm^2) and Reduced Size(13x5x3 mm, Bulk Surface Area≈ 2.4cm^2). The reaction kinetics were followed by measuring specimen weight loss as a function of time using a Cahn RH or Cahn 2000 microbalance.

Typical weight loss data for Large Size specimens at several temperatures between 600 and 900°C are presented in Figures 8 to 11. In this temperature range the weight losses are generally larger for the uninhibited composites. Additionally the shape of the weight loss curves are different between the inhibited and uninhibited materials. The uninhibited composites show an initial region with increasing slope followed by a second region which is linear. The inhibited specimens show the same two regions followed by a third region of decreasing slope. This three region behavior can be clearly seen for the data plotted for Reduced Size inhibited specimens over a range of temperatures in Figure 12. The third region is believed to result from boron oxides coating the remaining, unreacted composite and decreasing the rate. The apparent reaction rate in the third region decreases by two orders of magnitude with respect to the rate in the second region. However, this decrease may result partially from weight gains associated with formation of B_2O_3(See Figures 13 and 14). The interpretation of the weight change data is further complicated by possible evaporation of volatile boron-oxygen species(See Figures 15 and 16). The weight loss rates(measured from the linear portion of the weight loss-time curves) are plotted versus reciprocal temperature on a semilog plot in Figure 17. The rates are seen to fall into two regimes, as discussed previously. At temperatures below about 800°C the rates depend strongly on temperature which is typical of chemical reaction control. The activation energies obtained from this region were aproximately 48 kcal/mole for the uninhibited and 40 kcal/mole for the inhibited composites. The significance of the differences in activation energies is not clear since McKee[7] has reported a similar range for tests on uninhibited carbon-carbon. At

temperatures above about 800°C the rates become essentially independent of temperature which is typical of reaction control by diffusion control in the gas phase. Figures 18 and 19 show more detail of the rates in this range and the effects of flow rate and specimen size. The following observations may be made from these figures.

(i) The rates are faster for the uninhibited materials for a given specimen size and flow rate.

(ii) The rates increase with increasing flow rate for a given material and specimen size.

(iii) The rates increase with decreasing specimen size for a given material and flow rate.

The second two effects are related since local depletion of oxidant in the gas phase becomes significant for either large specimens or slow flow rates.

Characterization of Oxidized Composites

Figures 20 and 21 show the microstructures of CC 139E and CC 137E, respectively, after oxidation at 600°C in oxygen at a flow rate of 100 cm^3/min. In both cases the CVD carbon is degraded to a greater extent than the fibers and the exposed surface of the matrix, especially for CC 139E, is covered with porous nodules. Figure 22 shows CC 139E oxidized at 700°C. The upper micrograph shows the remnants of the CVD carbon layer and the middle and bottom micrographs clearly show the preferential removal of the matrix.

Figure 23 shows the structure of CC 137E after oxidation at 800°C along with oxygen, carbon and boron x-ray maps. This figure indicates that the slower oxidation rate of the inhibited composite(Figure 10) results from the formation of boron oxide which coats the composite during oxidation.

Figure 24 shows the structure of CC 137E which was oxidized at 950°C i.e. in the diffusion-controlled regime. The remaining carbon is covered with a glassy coating and the

lower micrograph indicates that substantial attack of the fibers, as well as the matrix, has occurred.

Figure 25 shows the structure of CC 139E after oxidation at 1100°C and a flow of 100 cm^3/min. Little or no matrix remains indicating selective removal of this constituent.The attack of the fibers was observed to affect the macroscopic shape of the specimen producing thinning of the leading edge. Figures 26 and 27 show the structures of CC 137E and CC 136E after oxidation at 1100°C. Attack of the fibers is evident and the two inhibited composites are coated with a glassy boron oxide film. The bottom micrograph of Figure 27 indicates cracking of this film which was observed to occur during cooling.

Figure 28 presents the density measured by helium adsorption and the apparent density of a number of specimens following oxidation to produce various amounts of weight loss. The apparent density(mass/bulk volume) decreases substantially with oxidation, especially for inhibited composites, while the measured density remains relatively constant. This results from the more rapid attack of the matrix relative to the fibers which leaves the macroscopic dimensions of the composite unchanged even though a substantial amount of the matrix between the fibers has been oxidized away. This effect is accentuated for the inhibited composites since the fibers become coated with boron compounds which restrict access of oxygen whereas the attack of the uninhibited composites is more uniform. Measurement of the surface area of the specimens, using the BET method with nitrogen gas, indicates an initial value of approximately 2.2 m^2/g for both the inhibited and uninhibited composites. In most cases this value increases to as much as 4 m^2/g after oxidation. This increase is believed to result from oxidation of the outer CVD carbon layer which exposes the more porous composite and hence the increase in surface area as measured by the BET method.

Characterization of Coated Composites

The as-processed structures of CC 137E with several coatings are illustrated in Figures 29 to 31. The characterization of these materials is continuing but one common feature is cracking of the SiC coating.

WORK TO BE PERFORMED DURING THE THIRD YEAR OF THE PROGRAM

Work during the third year of this program will concentrate on characterizing the oxidation behavior of the coated composites and on evaluating the effects of water vapor on the oxidation behavior of Carbon-Carbon composites. An apparatus has been constructed which will allow weight change measurements to be made in atmospheres containing well-controlled amounts of water vapor. Particular emphasis will be placed on the interactions between water vapor and the boron inhibitors.

REFERENCES

1. K. L. Luthra, "Oxidation of Carbon/Carbon Composites - A Theoretical Analysis", General Electric Corporate Research and Development Report No. 866rd096, May, 1987; Schenectady, New York.
2. D. W. McKee, "Chemistry and Physics of Carbons", Vol. 16; P. L. Walker, Jr. and P. A. Thrower eds.; Marcel Dekker, New York, 1981.
3. D. W. McKee, Carbon, 24, 737(1986).
4. P. Ehrburger, P. Baranne, and J. Lakaye, Carbon, 24, 1986.
5. V. S. Dergunova, A. V. Emyashev, G. A. Kravetskii, and V.N. Sushin, "High-Temperature Coatings on Graphite", in High Temperature Protective Coatings, A. I. Borisenko ed., Translated from Russian, National Bureau of Standards, Washington, D. C., 1986, p.127.
6. R. Keiser, "Oxidation Protection for High Strength Carbon-Carbon Composites", Report AFWAL-TR-82-4060, Prepared by Garrett Turbine Engine Co., Phoenix, Arizona for WPAFB Materials Laboratory, WPAFB, Ohio, June, 1982.
7. D. W. McKee, Carbon, 25, 551(1987).

Figure 1. Plots of various oxidation rates of carbon. Acceptable rates of carbon loss for long-term and short-term applications are based on 12.5 mils in 2000 and 20 hours, respectively (ref. 1).

CARBON CARBON OXIDATION RESULTS

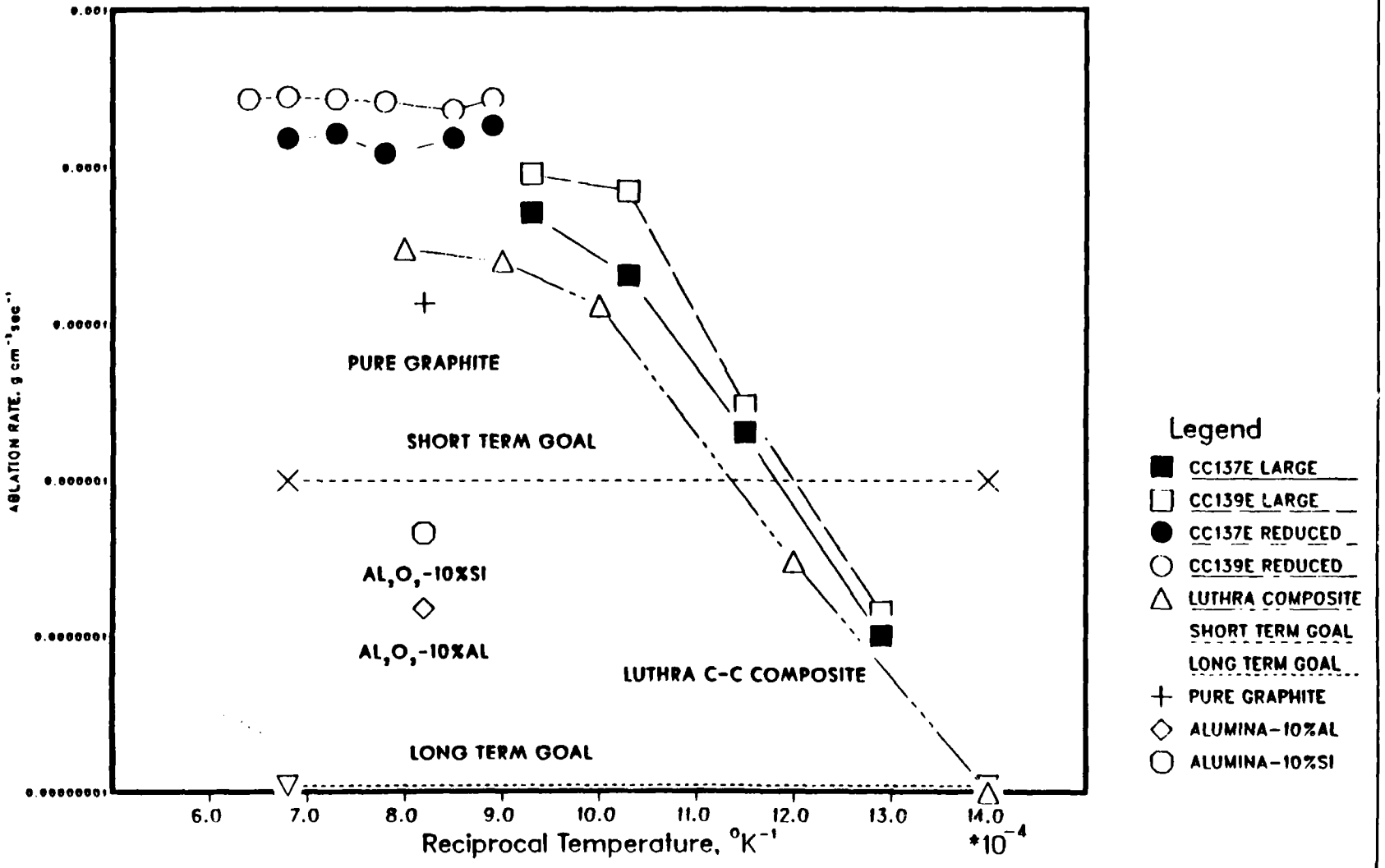

Figure 2. Initial structure of CC 139E. The top micrograph shows the CVD carbon coating and the underlying composite through the fissures in the coating. The fragmented nature of the surface results from unequal thermal expansion of the fibers and coating during processing. This figure also shows that densification of the composite by CVD is confined to regions near the surface. The middle and bottom micrographs show through-thickness and planar sections of the composite, respectively.


S

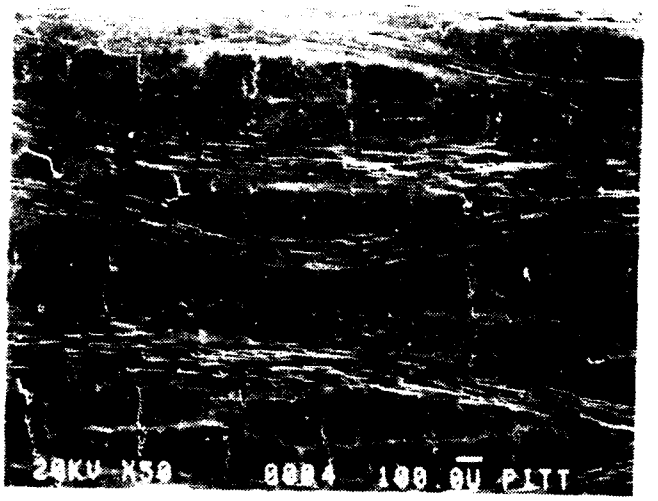
20KV X50 0004 100.0U PITT


20KV X10 0006 100 0U PITT

Figure 3. Optical micrographs of CC 136E(both at the same magnification). The top micrograph shows the CVD carbon layer at the surface and its penetration into the composite. The bottom micrograph shows B_4C particles among the fibers.

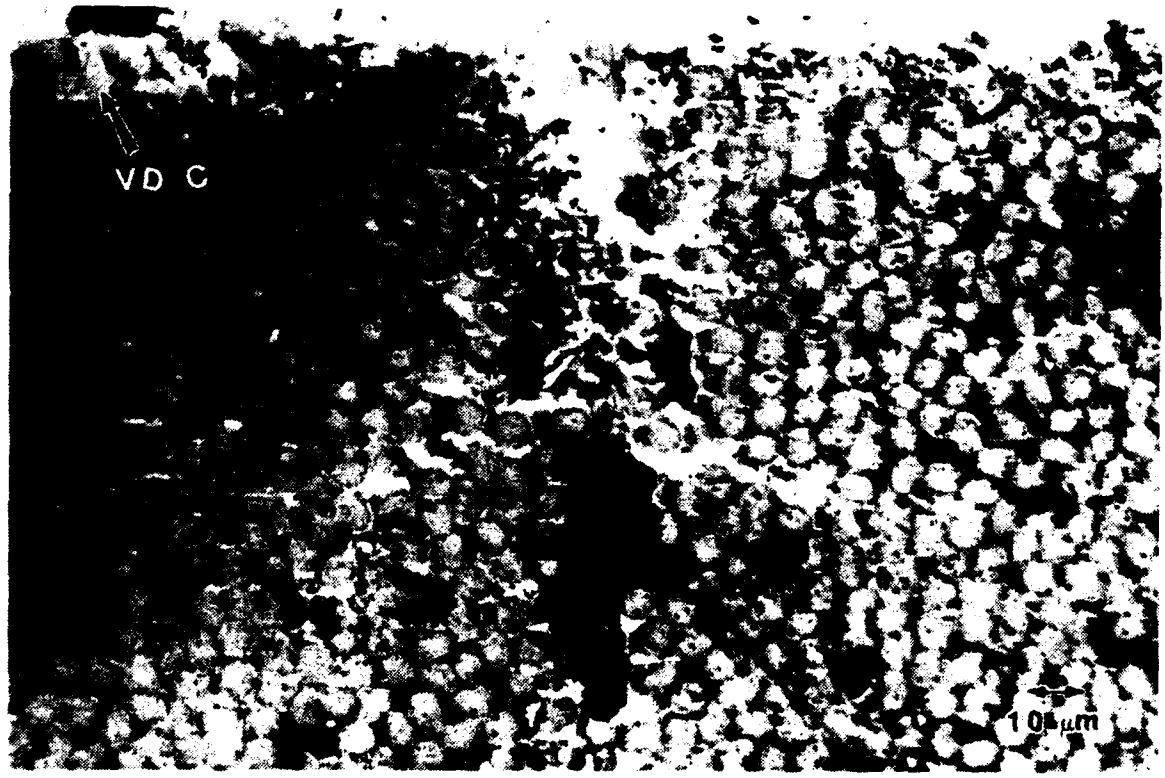
VD C
10 µm

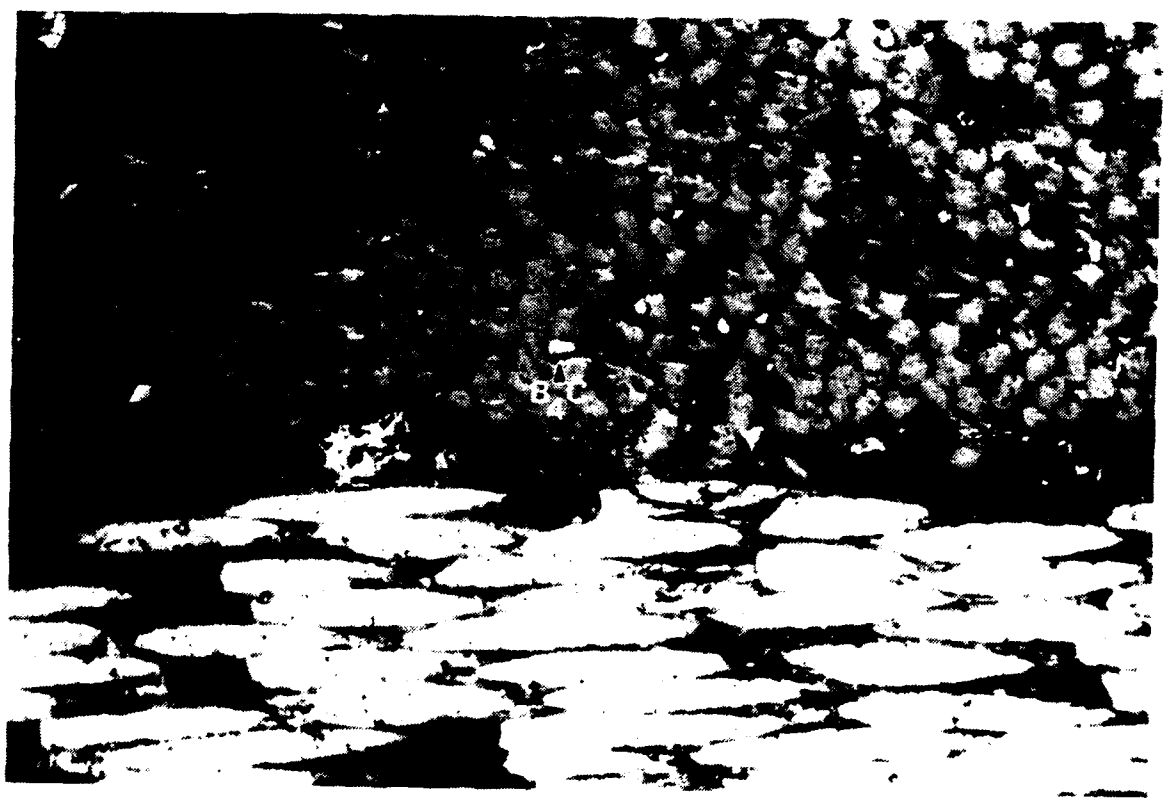
B C

Figure 4. Micrograph and accompanying boron x-ray map for a B_4C particle in as-processed CC 136E.


12KV X3000 0124 10.0U PITT

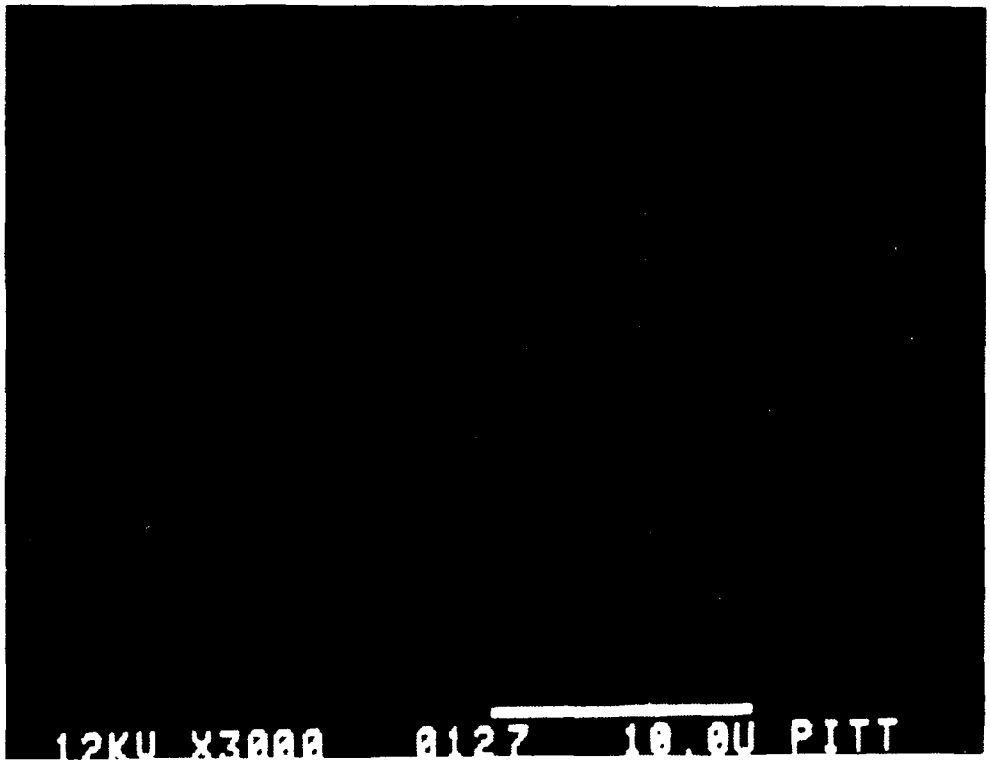
12KV X3000 0127 10.0U PITT

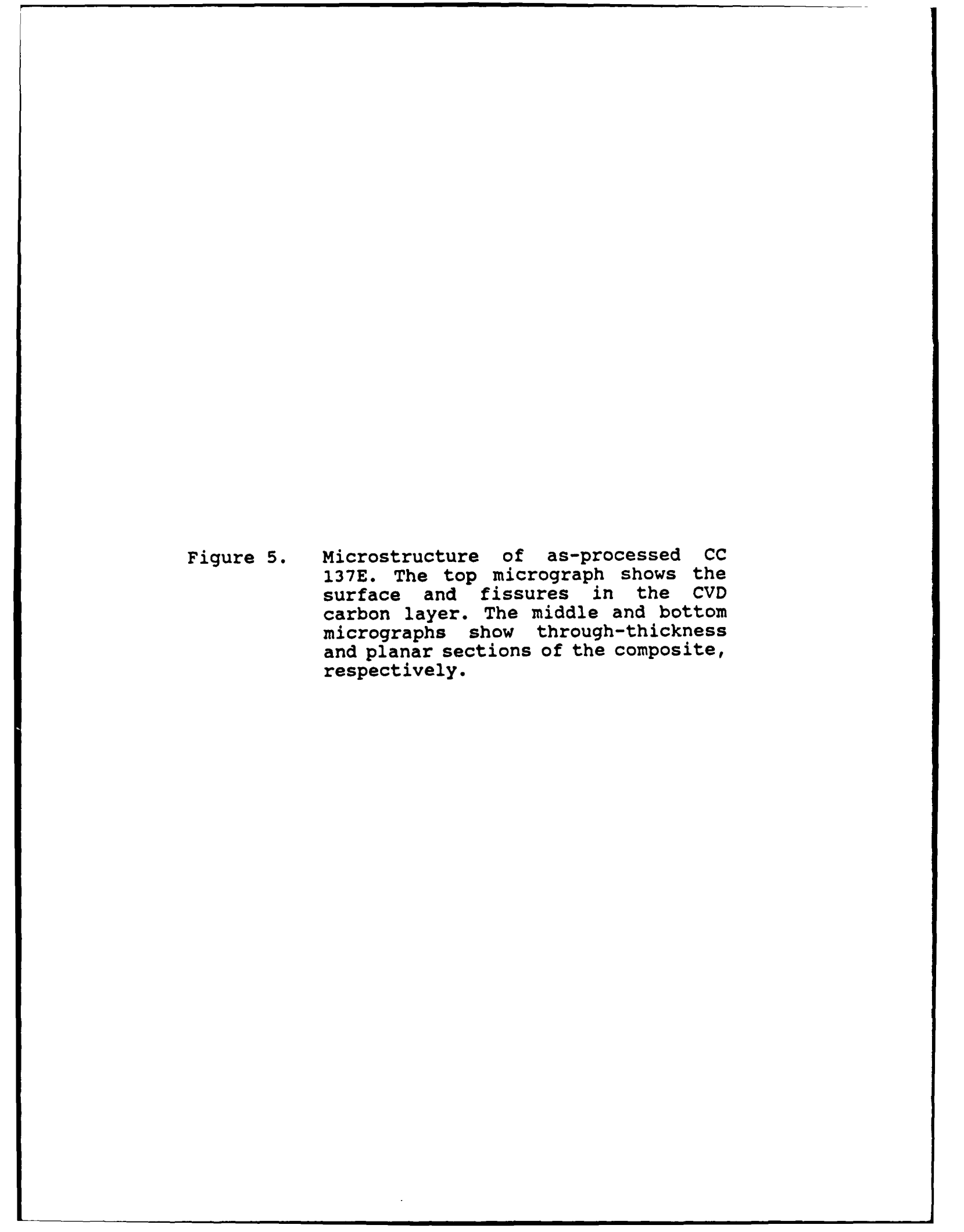

Figure 5. Microstructure of as-processed CC 137E. The top micrograph shows the surface and fissures in the CVD carbon layer. The middle and bottom micrographs show through-thickness and planar sections of the composite, respectively.

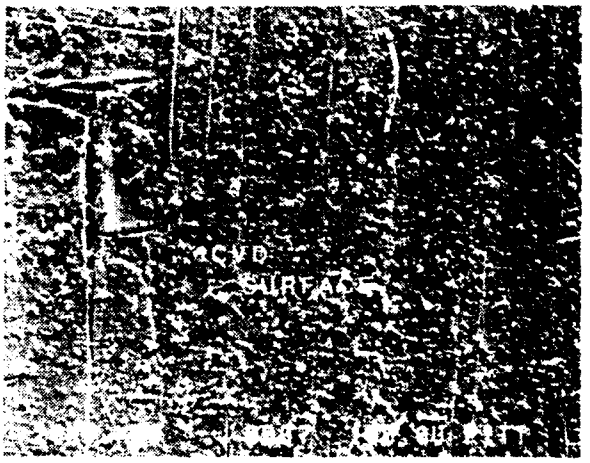
CVD
SURFACE

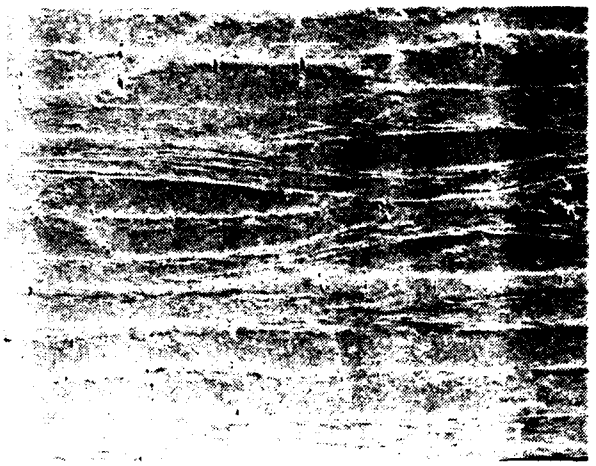

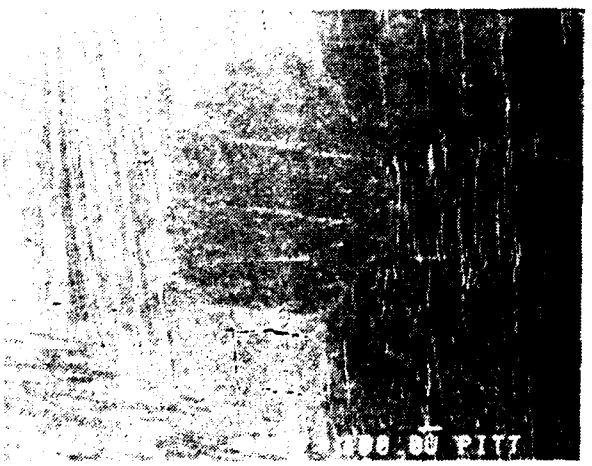
PIT

Figure 6. Transmission electron micrograph of as-processed CC 137E. The top left is a bright-field micrograph of a region containing both fiber and matrix. The SAD ring pattern(at right) indicates the structures are microcrystalline. Intensity maxima in 002 and 004 orientations occur normal to the fiber axis. The bottom left is a dark-field image produced using the 002 spot.

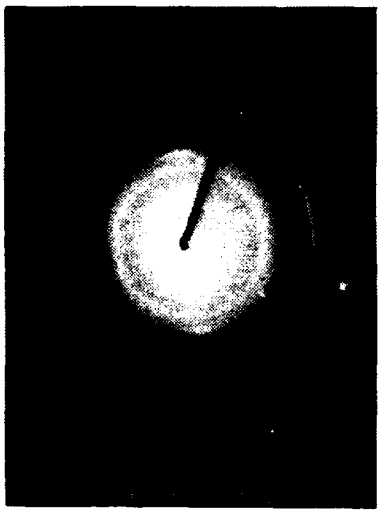

Figure 7. Bright field micrograph of the matrix in as-processed CC 137E.


137E
X85K 100nm

Figure 8. Weight loss vs time data for various composites at 600°C.

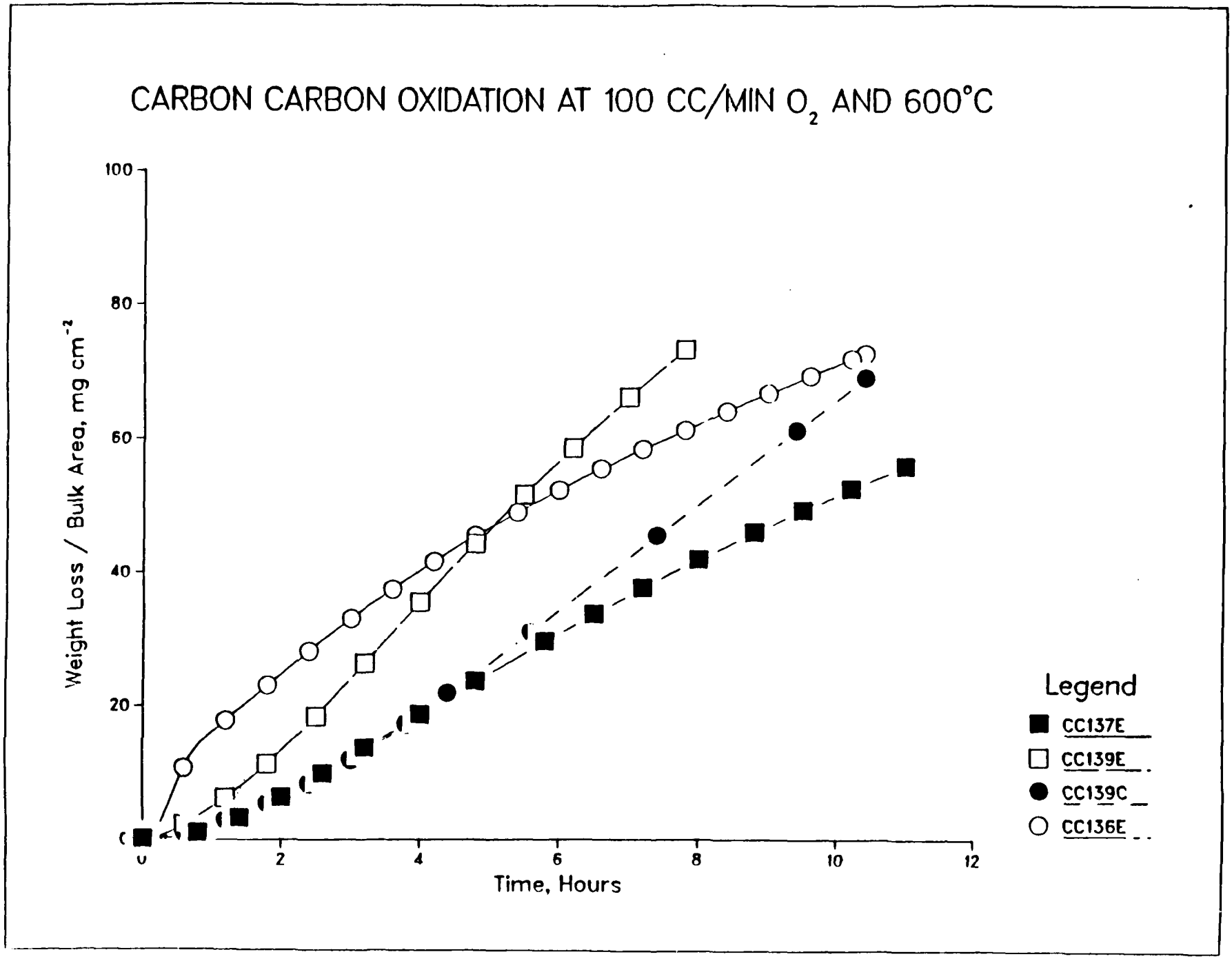
CARBON CARBON OXIDATION AT 100 CC/MIN O_2 AND 600°C
Weight Loss / Bulk Area, mg cm^{-2}
100
80
60
40
20
0
2
4
6
8
10
12
Time, Hours
Legend
CC137E
CC139E
CC139C
CC136E

Figure 9. Weight loss vs time data for various composites at 700°C.

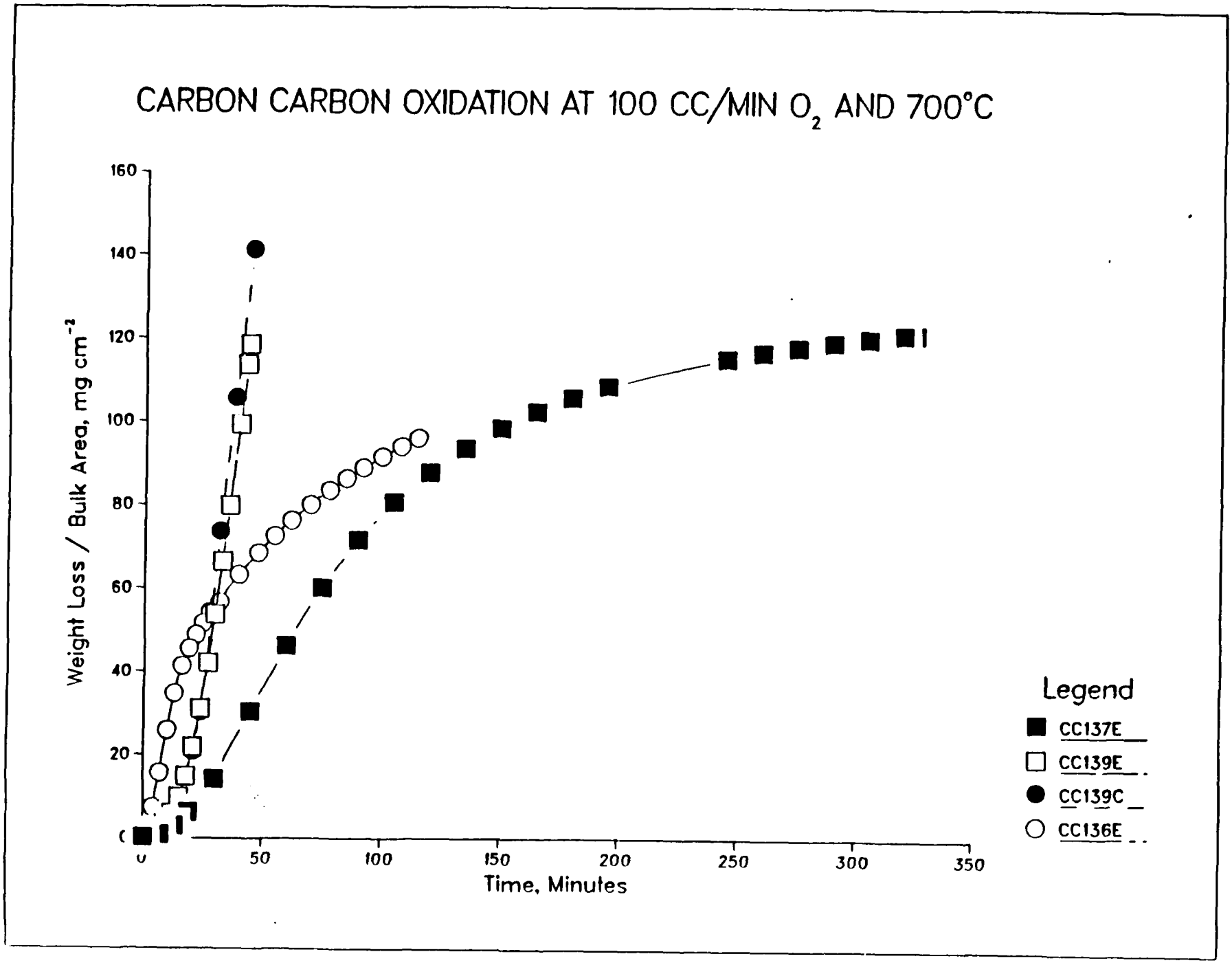
CARBON CARBON OXIDATION AT 100 CC/MIN O_2 AND 700°C
Weight Loss / Bulk Area, mg cm^{-2}
160
140
120
100
80
60
40
20
0
50
100
150
200
250
300
350
Time, Minutes
Legend
CC137E
CC139E
CC139C
CC136E

Figure 10. Weight loss vs time data for various composites at 800°C.

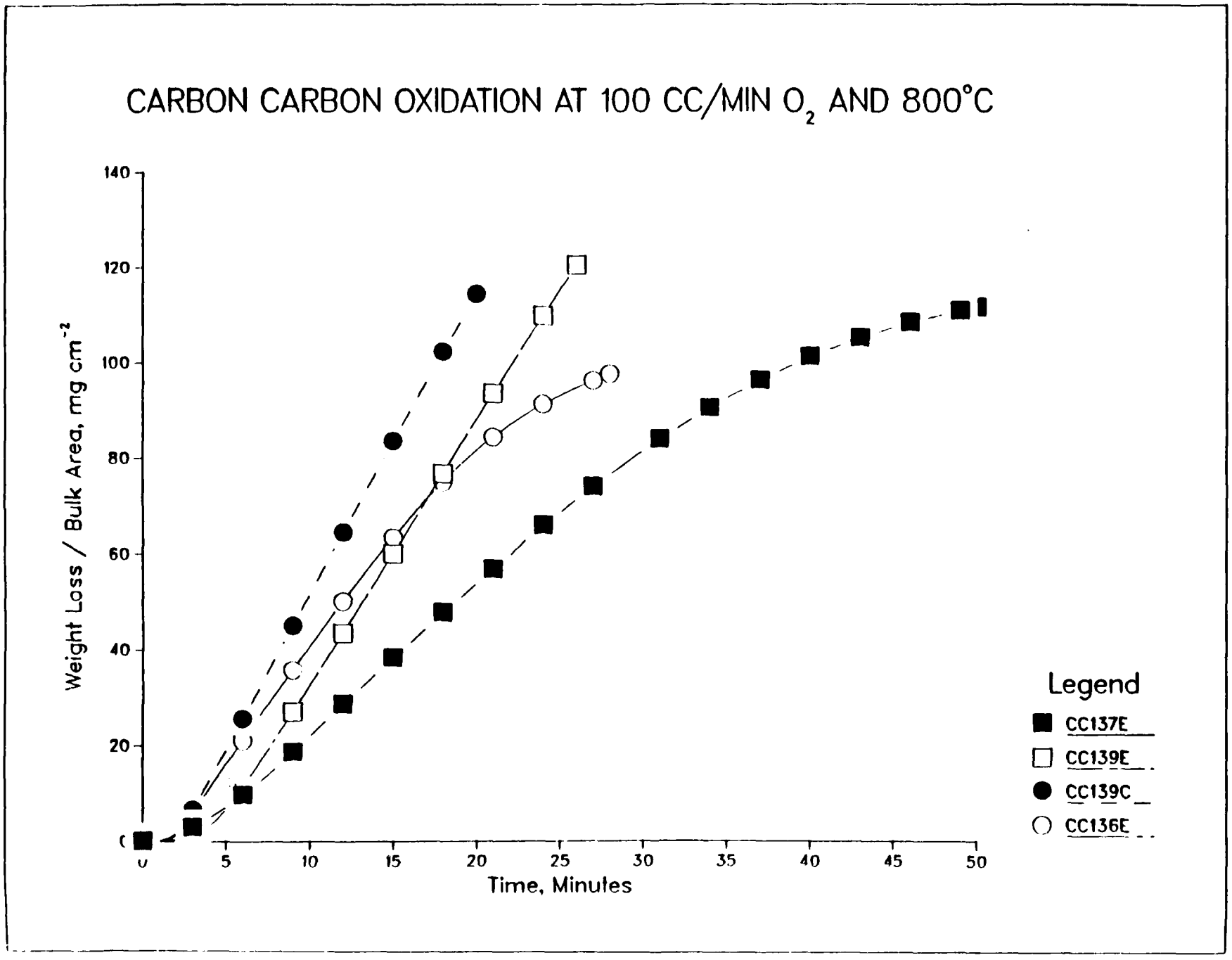
CARBON CARBON OXIDATION AT 100 CC/MIN O_2 AND 800°C
Weight Loss / Bulk Area, mg cm^{-2}
140
120
100
80
60
40
20
0
5
10
15
20
25
30
35
40
45
50
Time, Minutes
Legend
CC137E
CC139E
CC139C
CC136E

Figure 11. Weight loss vs time data for various composites at 900°C.

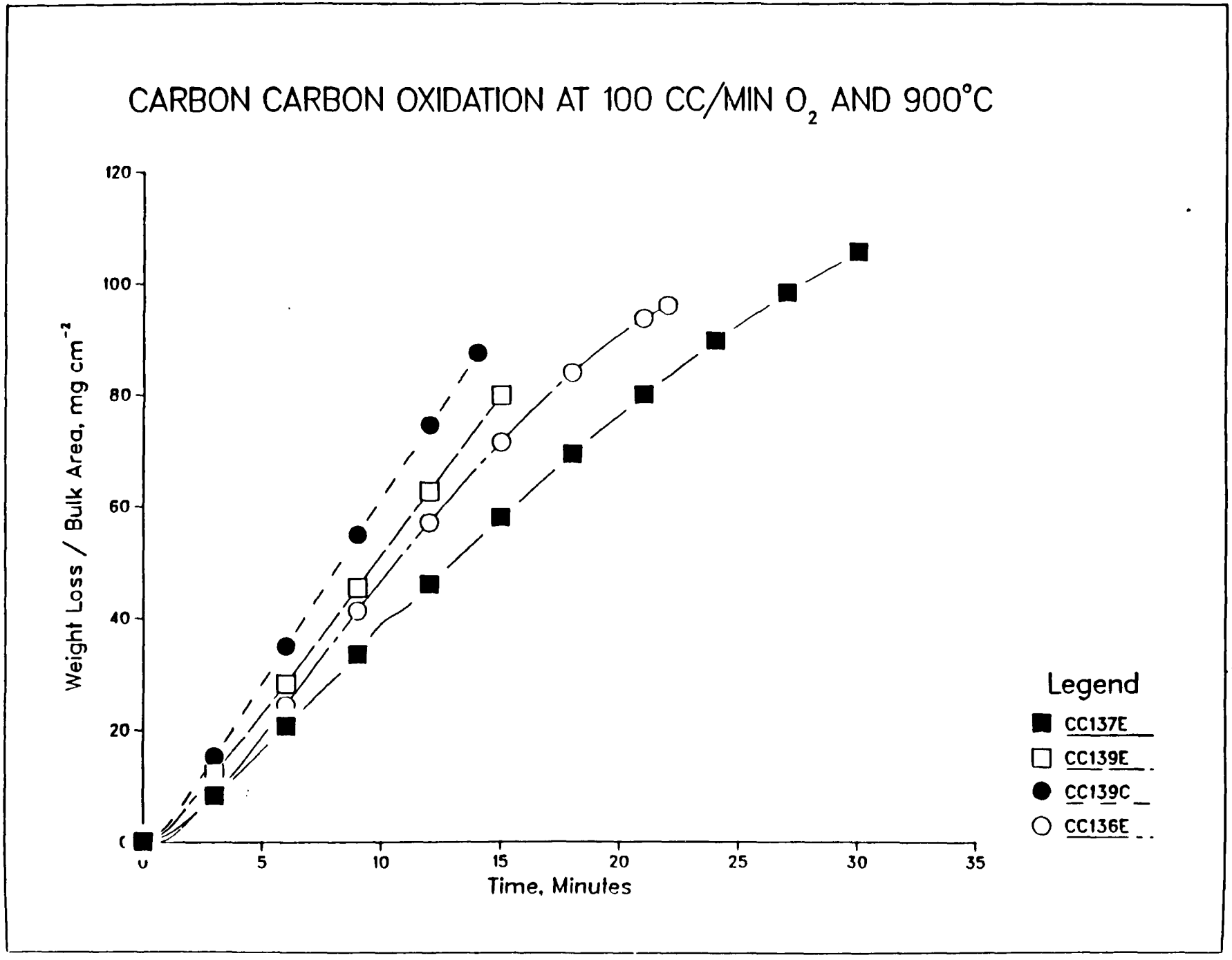
CARBON CARBON OXIDATION AT 100 CC/MIN O_2 AND 900°C
Weight Loss / Bulk Area, mg cm^{-2}
120
100
80
60
40
20
0
0
5
10
15
20
25
30
35
Time, Minutes
Legend
CC137E
CC139E
CC139C
CC136E

Figure 12. Weight loss vs time data for CC 137E(reduced) specimens at various temperatures.

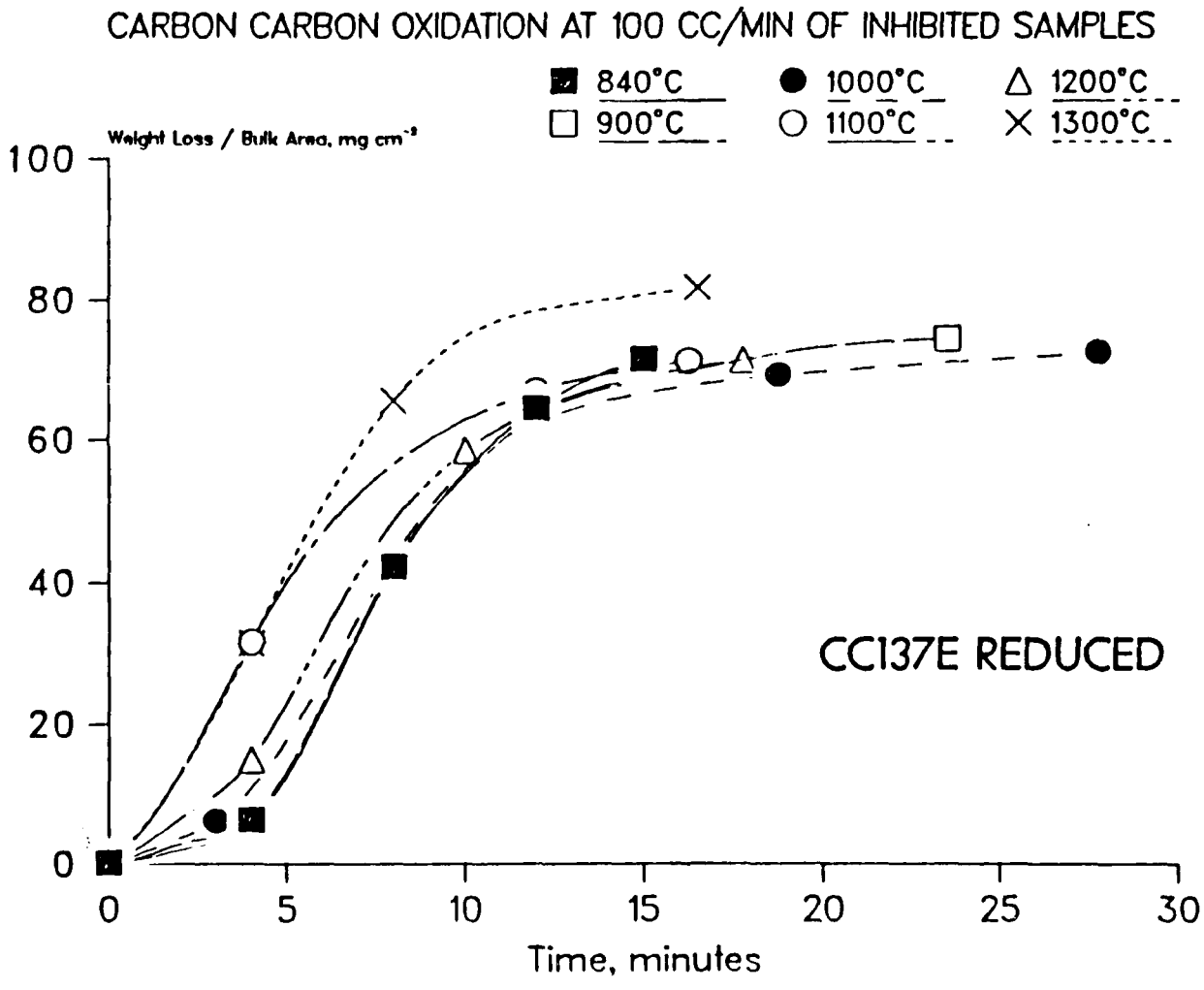
CARBON CARBON OXIDATION AT 100 CC/MIN OF INHIBITED SAMPLES
840°C
900°C
1000°C
1100°C
1200°C
1300°C
Weight Loss / Bulk Area, mg cm⁻²
100
80
60
40
20
0
0
5
10
15
20
25
30
Time, minutes
CC137E REDUCED

Figure 13. Isothermal stability diagram describing phase equilibria in the carbon-oxygen-boron system at 1250K.

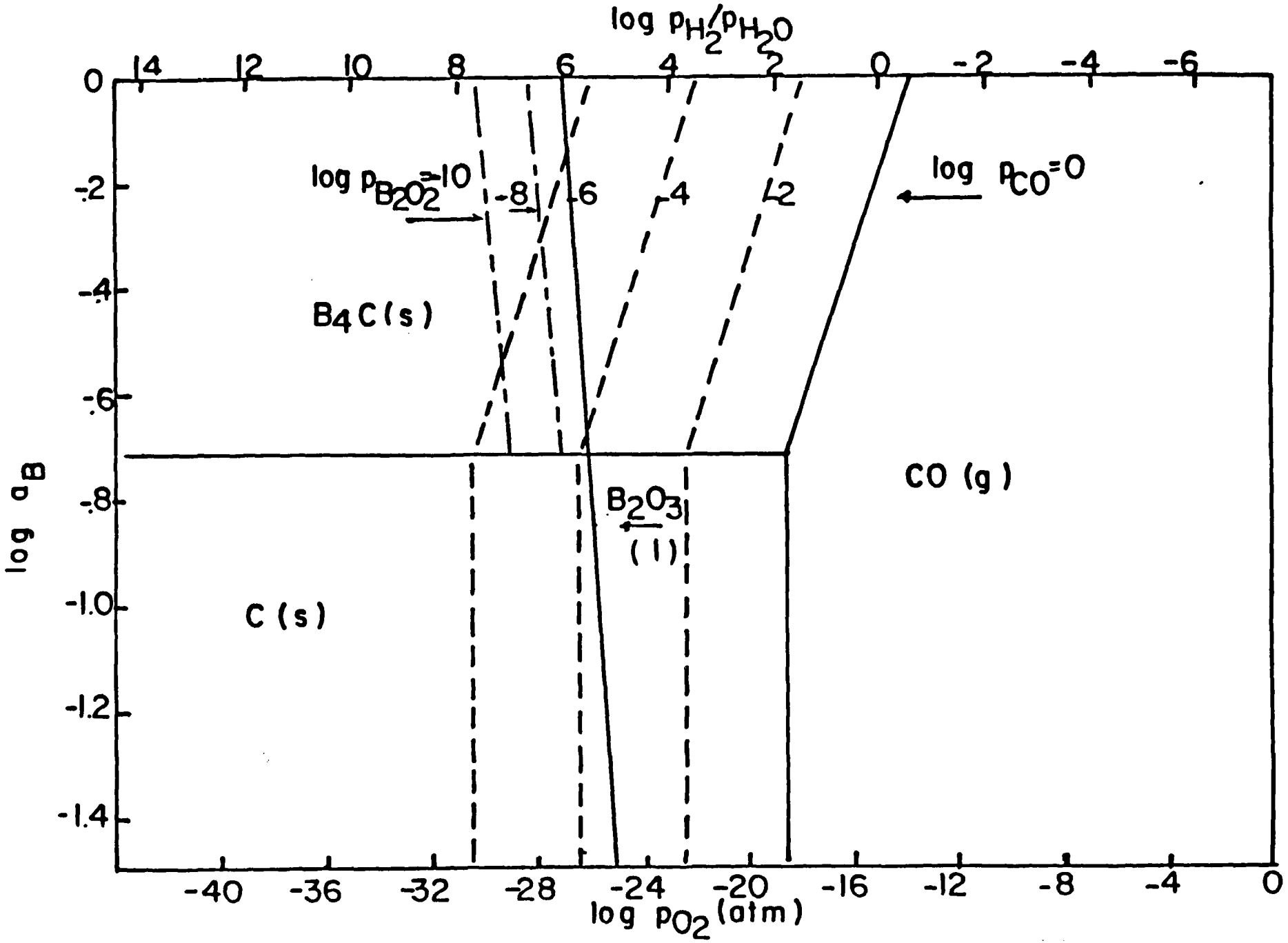
log p_{H_2}/p_{H_2O}
14
12
10
8
6
4
2
0
-2
-4
-6
log $p_{B_2O_2}$=10
8
6
4
2
log p_{CO}=0
B_4C(s)
B_2O_3
(l)
CO (g)
C (s)
log a_B
0
-2
-4
-6
-8
-1.0
-1.2
-1.4
-40
-36
-32
-28
-24
-20
-16
-12
-8
-4
0
log p_{O_2}(atm)

Figure 14. Isothermal stability diagram describing phase equilibria in the carbon-oxygen-boron system at 1450K.

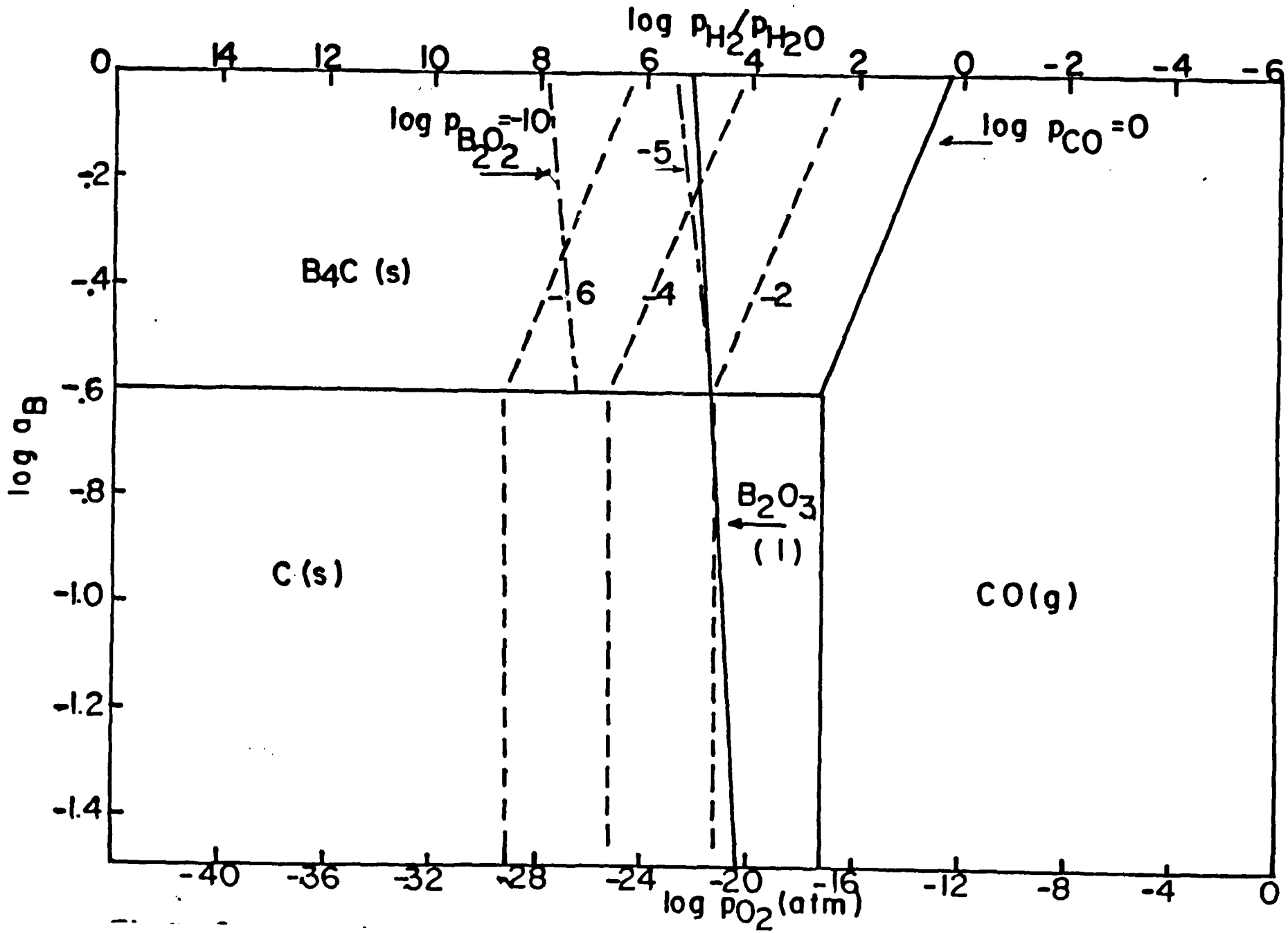
log p_{H_2}/p_{H_2O}
0
14
12
10
8
6
4
2
0
-2
-4
-6
log $p_{B_2O_2}$=-10
-5
log p_{CO}=0
-2
B4C (s)
-6
-4
-2
-.4
-.6
log a_B
-.8
B_2O_3
(l)
C (s)
CO(g)
-1.0
-1.2
-1.4
-40
-36
-32
-28
-24
-20
-16
-12
-8
-4
0
log p_{O_2}(atm)

Figure 15. Vapor species diagram for the boron-oxygen and silicon-oxygen systems at 1250K.

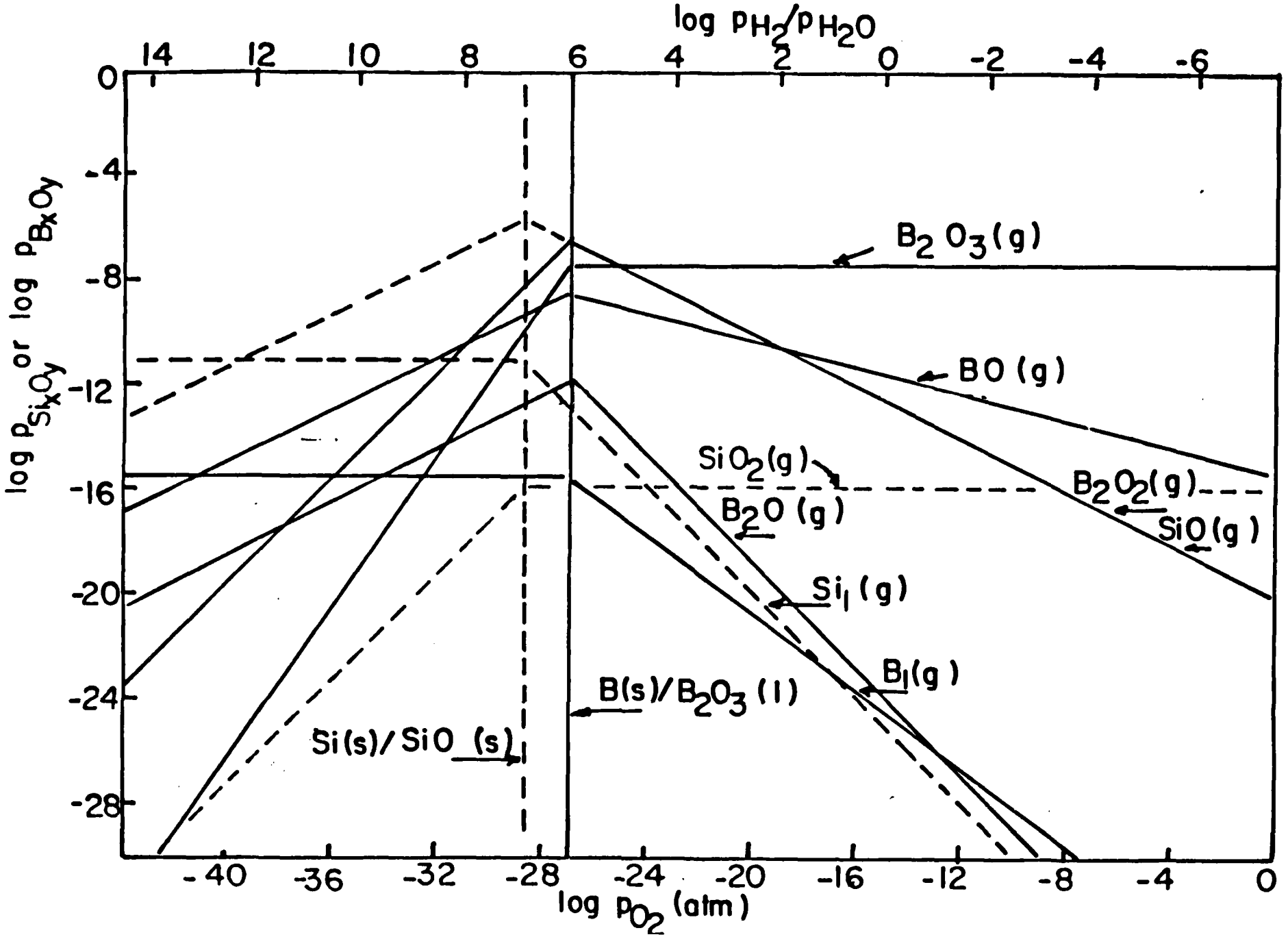
log p_{H_2}/p_{H_2O}
14
12
10
8
6
4
2
0
-2
-4
-6
0
-4
-8
-12
-16
-20
-24
-28
log $p_{Si_xO_y}$ or log $p_{B_xO_y}$
$B_2O_3(g)$
BO (g)
$SiO_2(g)$
$B_2O_2(g)$
B_2O (g)
SiO (g)
Si_1 (g)
B_1 (g)
B(s)/B_2O_3 (l)
Si(s)/SiO (s)
-40
-36
-32
-28
-24
-20
-16
-12
-8
-4
0
log p_{O_2} (atm)

Figure 16. Vapor species diagram for the boron-oxygen and silicon-oxygen systems at 1450K.

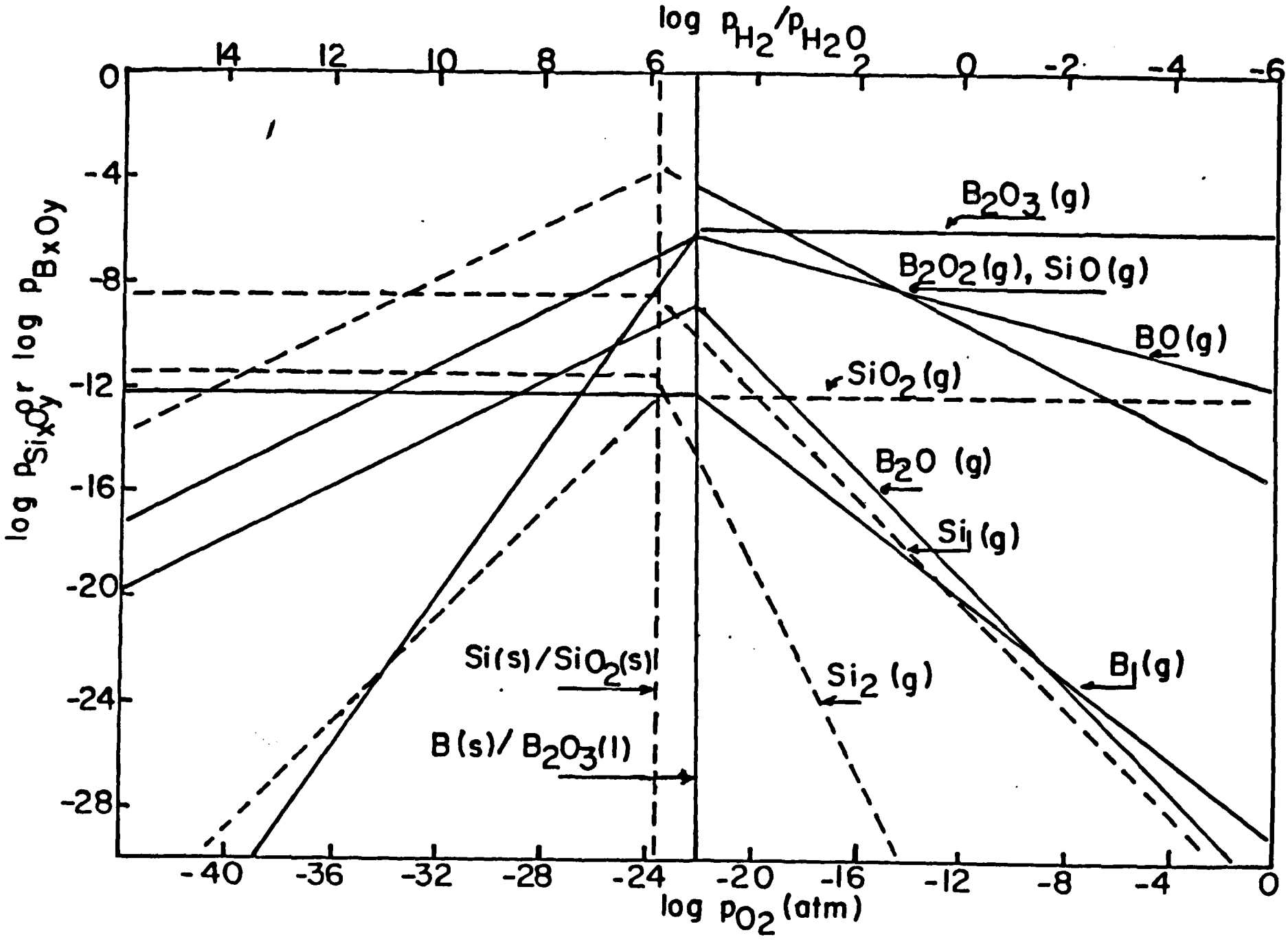
log p_{H_2}/p_{H_2O}
14
12
10
8
6
4
2
0
-2
-4
-6
0
-4
-8
-12
-16
-20
-24
-28
log $p_{Si_xO_y}$ or log $p_{B_xO_y}$
B_2O_3 (g)
B_2O_2 (g), SiO (g)
BO (g)
SiO_2 (g)
B_2O (g)
Si (g)
B_1 (g)
Si_2 (g)
Si (s) / SiO_2 (s)
B (s) / B_2O_3 (l)
-40
-36
-32
-28
-24
-20
-16
-12
-8
-4
0
log p_{O_2} (atm)

Figure 17. Arrhenius plot of the oxidation rates of various composites.

CARBON CARBON OXIDATION AT 100 CC/MIN

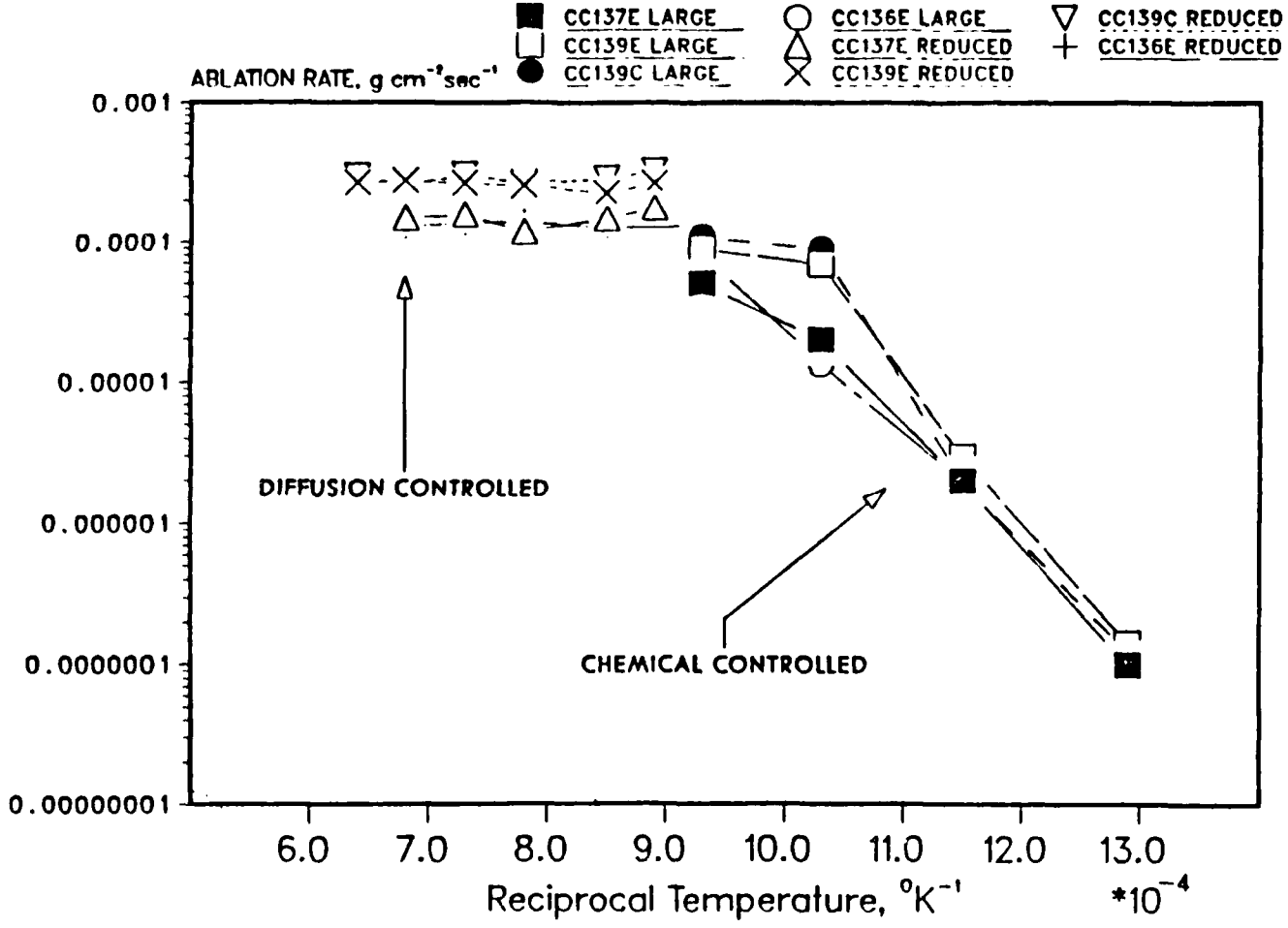

Figure 18. Arrhenius plot of the oxidation rates of various composites in the gaseous diffusion-controlled regime showing the effects of specimen size and flow rate.

CARBON CARBON OXIDATION AT 100 AND 550 CC/MIN

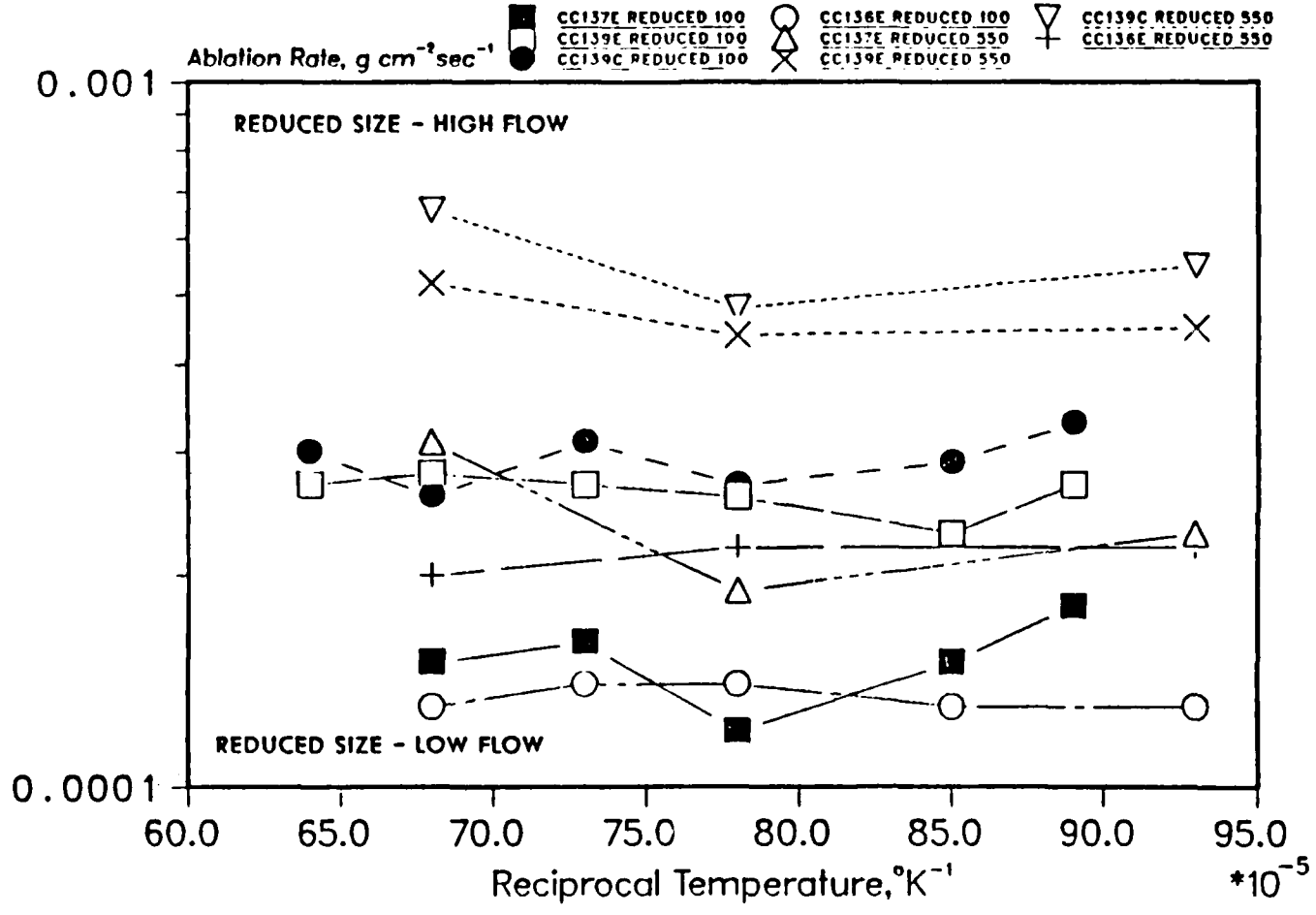

Figure 19. Arrhenius plot of the oxidation rates of various composites in the gaseous diffusion-controlled regime for an oxygen flow rate of 550 cm^3/min showing the effect of specimen size.

CARBON CARBON OXIDATION AT 550 CC/MIN

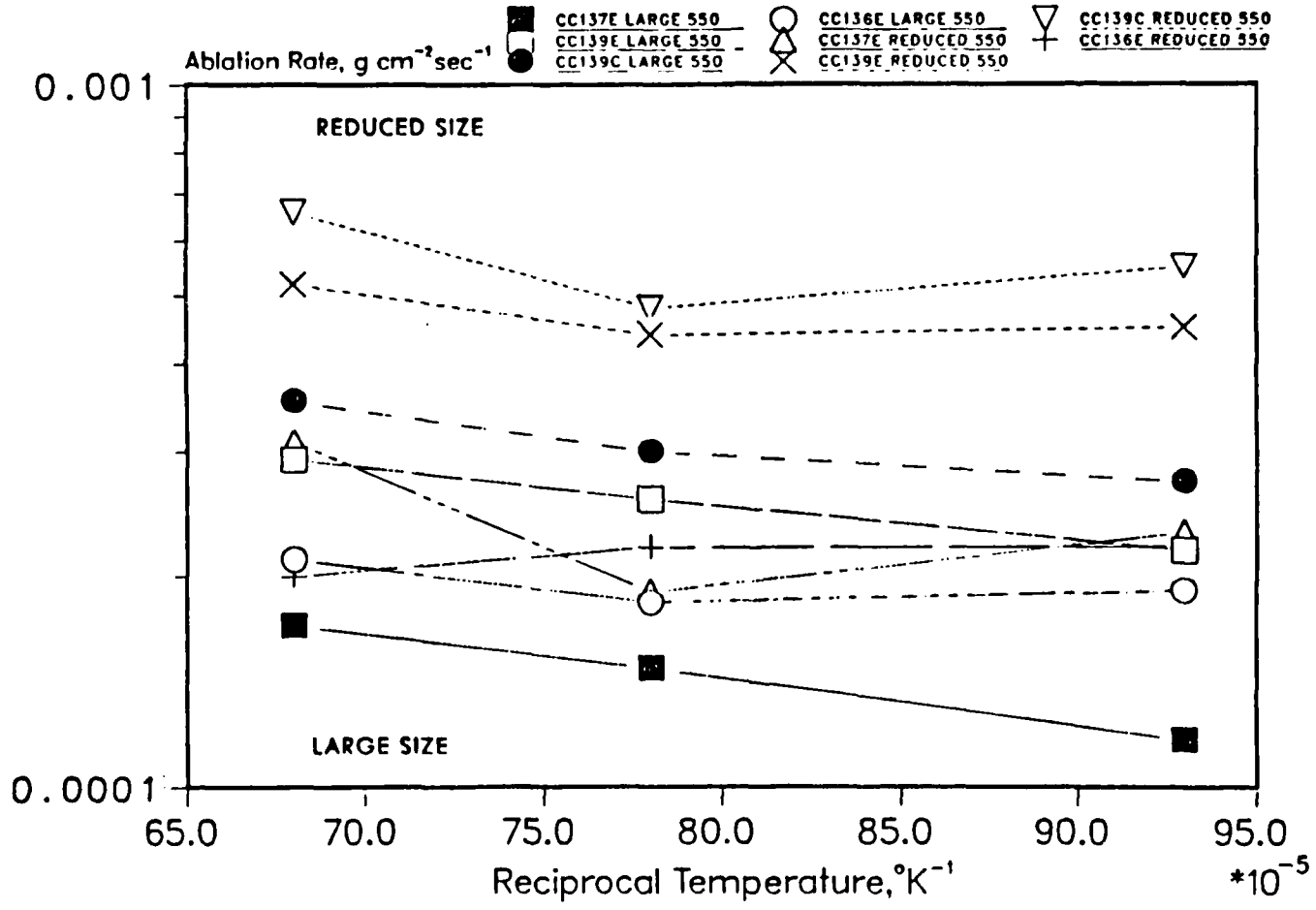

Figure 20. Structure of CC 139E after oxidation at 600°C and a flow rate of 100 cm^3/min. The top micrograph shows the matrix to have a nodular morphology. The bottom micrograph(taken at higher magnification) shows the porosity developed in this region.

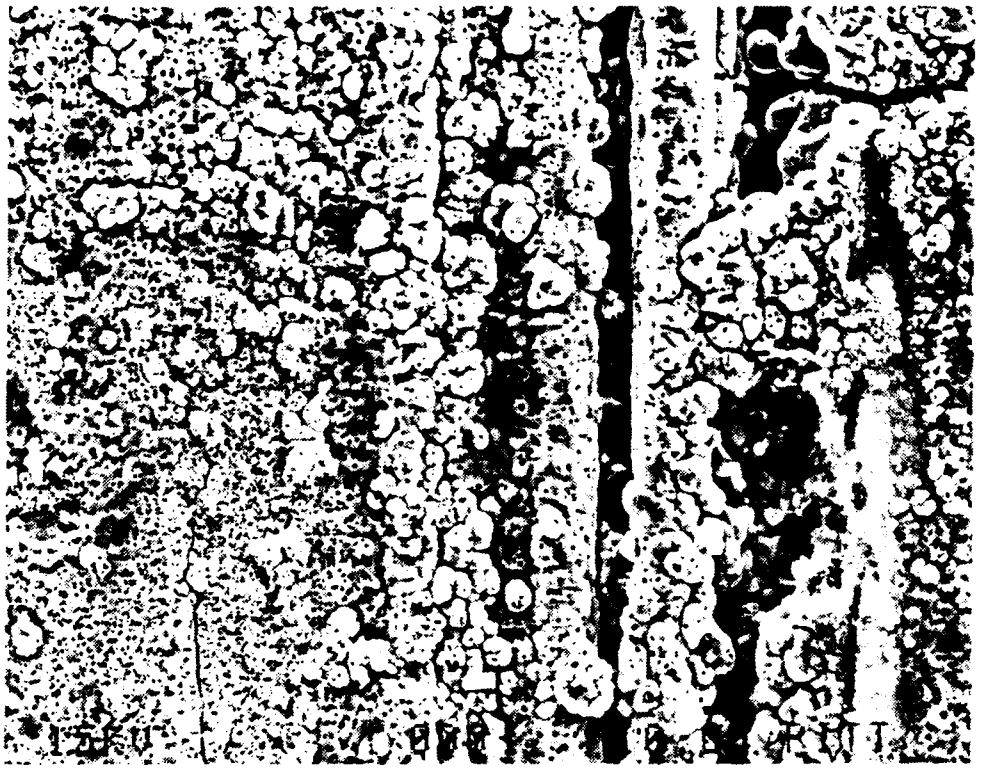

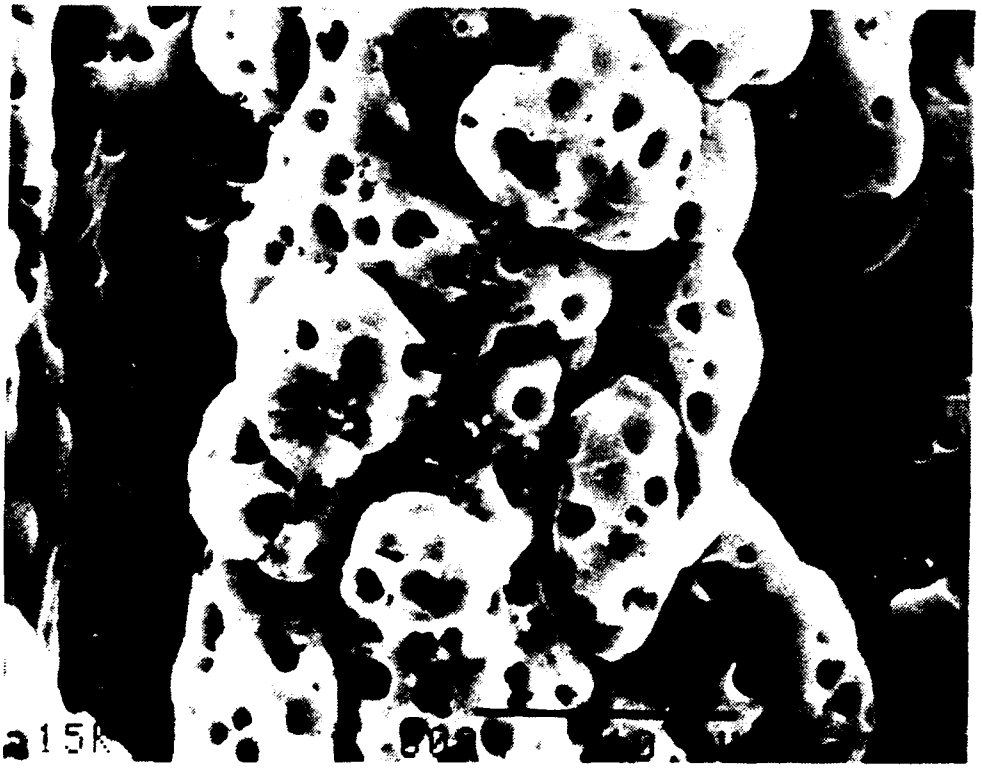

Figure 21. Structure of CC 137E after oxidation at 600°C and a flow rate of 100 cm^3/min.

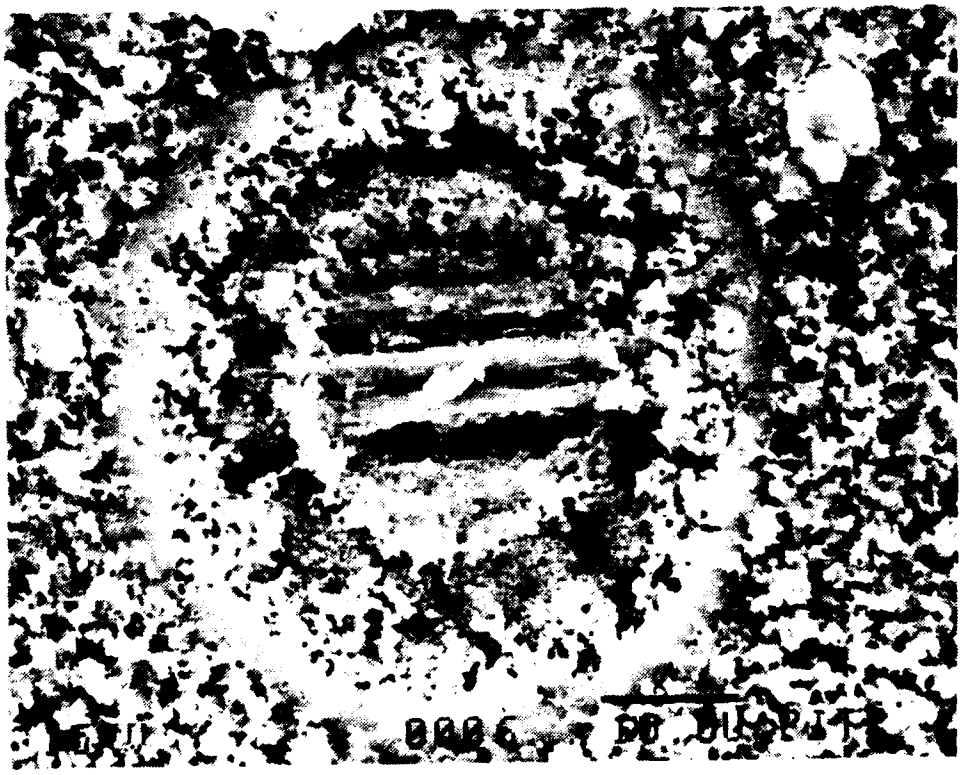

Figure 22. Structure of CC 139E after oxidation at 700°C and a flow rate of 100 cm^3/min.The top micrograph shows a region of the CVD carbon coating remaining on the surface. The middle micrograph shows the exposed fibers at higher magnification in a region where they have been only slightly attacked. The lower micrograph shows a region of more extensive fiber attack.

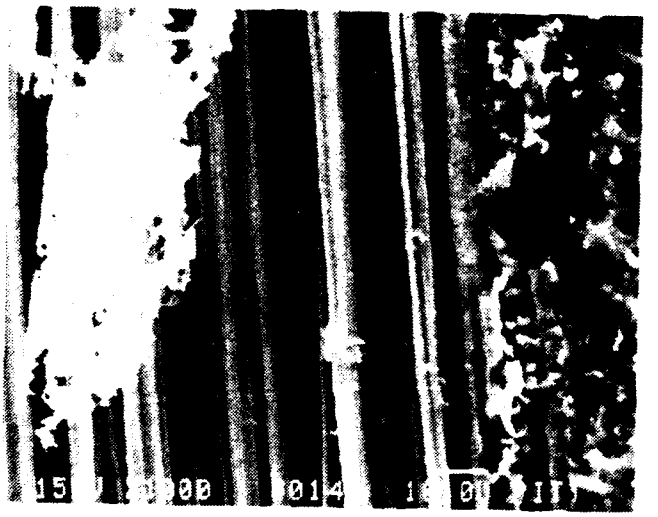

Figure 23. Micrograph of boron oxide formation on CC 137E after oxidation at 800°C and a flow rate of 550 cm^3/min. Carbon, oxygen, and boron x-ray maps accompany the micrograph.


D


C


B

Figure 24. Structure of CC 137E after oxidation at 950°C and a flow rate of 14 cm^3/min. The top micrograph shows a porous, plate-like structure of the carbon plys covered by a thin glassy coating. The bottom micrograph shows the attack of the fibers in a single ply at higher magnification.

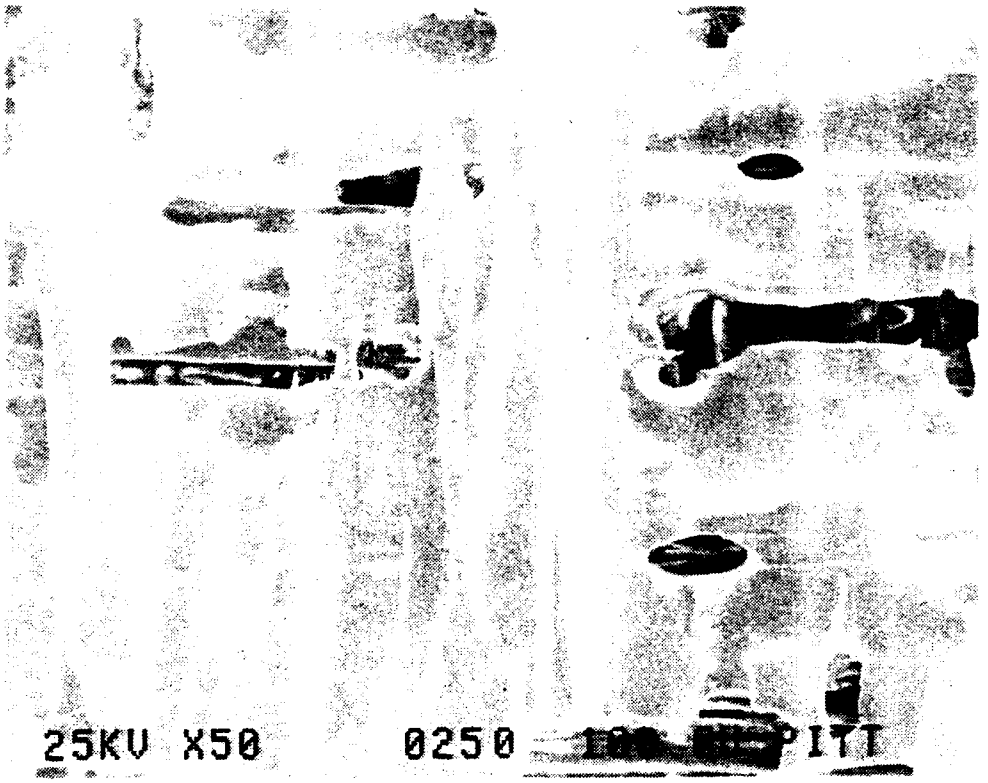
25KV X50 0250 PITT

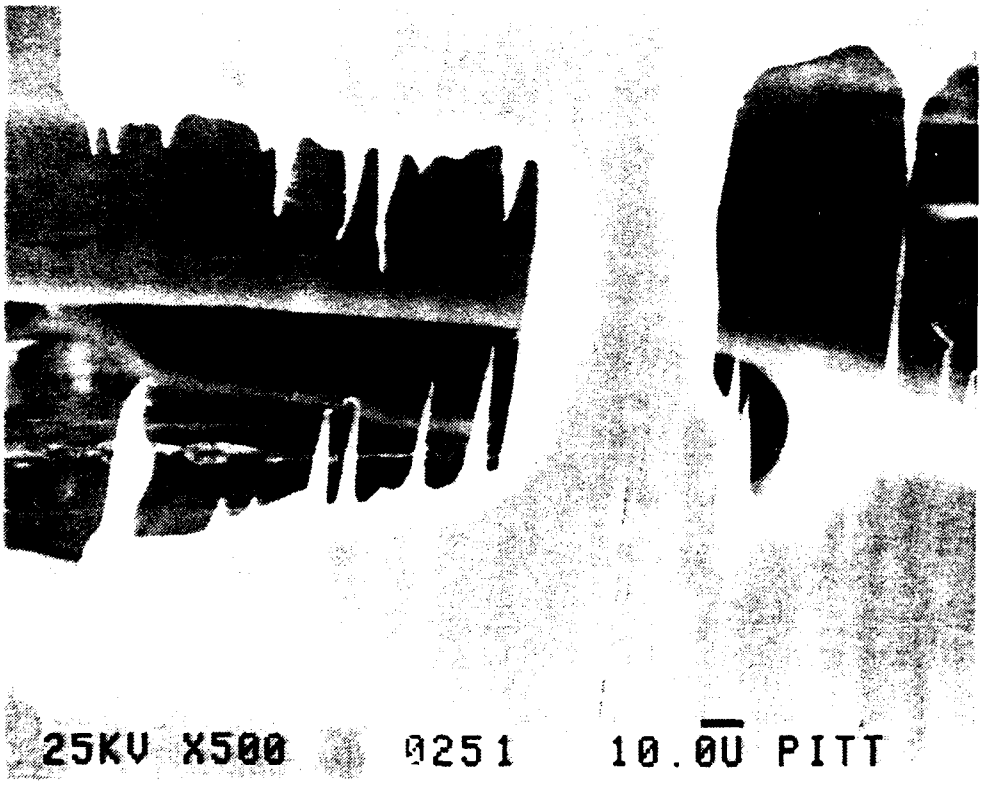
25KV X500 0251 10.0U PITT

Figure 25. Structure of CC 139E after oxidation at 1100°C and a flow rate of 100 cm^3/min showing completely exposed fibers.

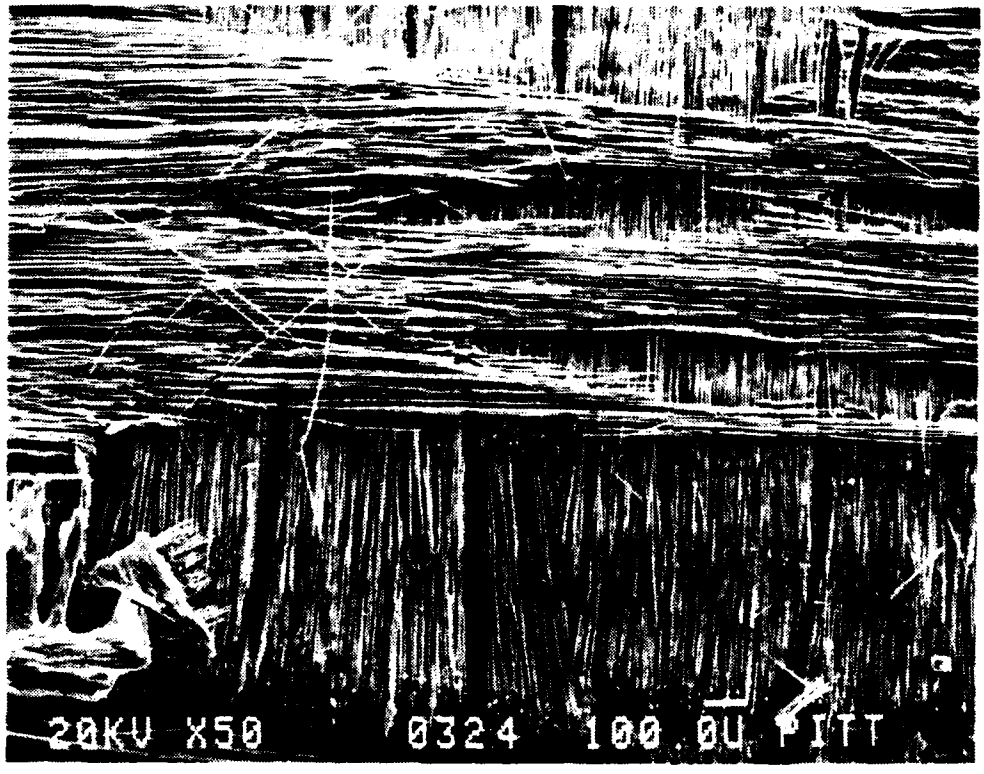
20KV X50 0324 100.0U PITT

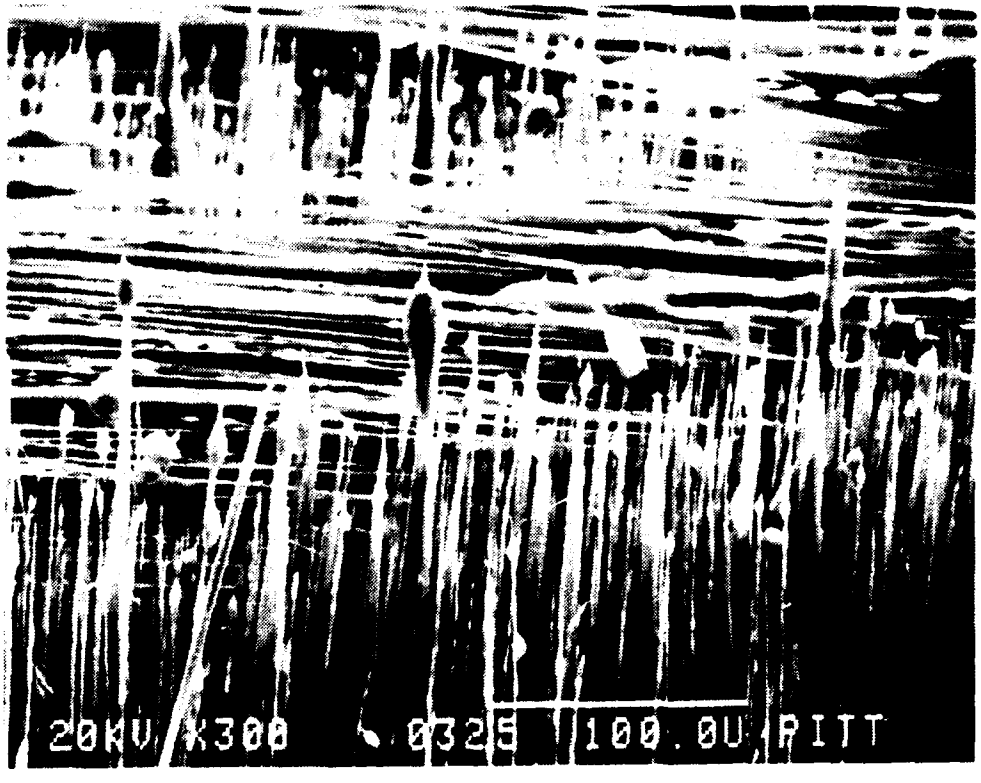
20KV X300 0325 100.0U PITT

Figure 26. Structure of CC 137E after oxidation at 1100°C and a flow rate of 100 cm^3/min showing the glassy coating formed over sections of the composite.


20KV X50
100.0U PIT

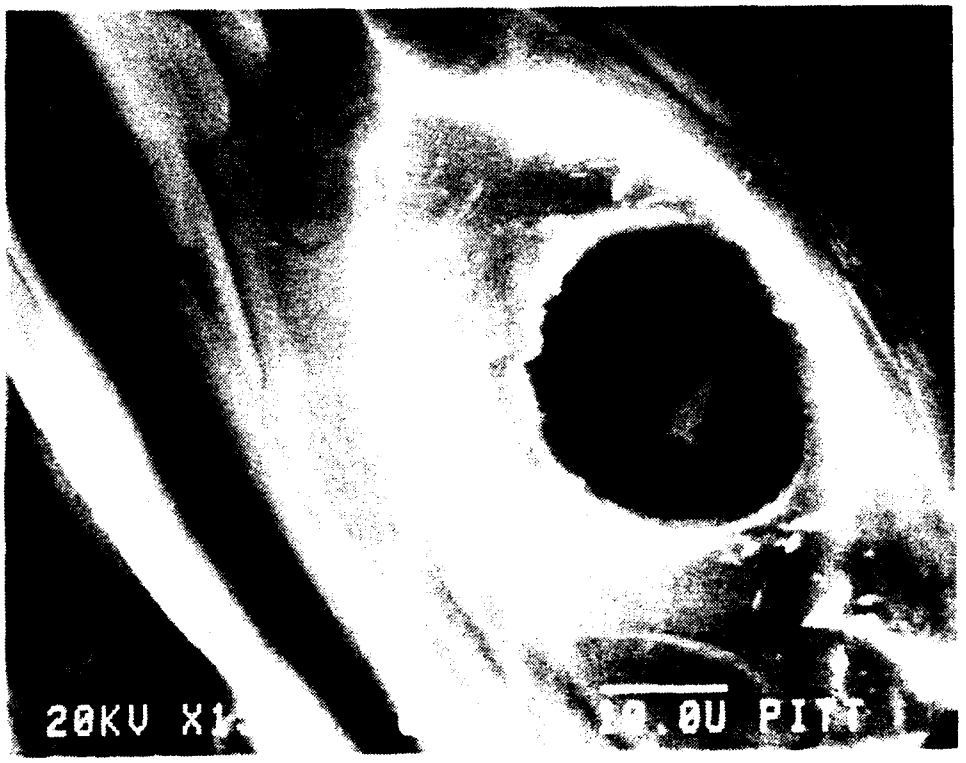
20KV X1
0.0U PIT

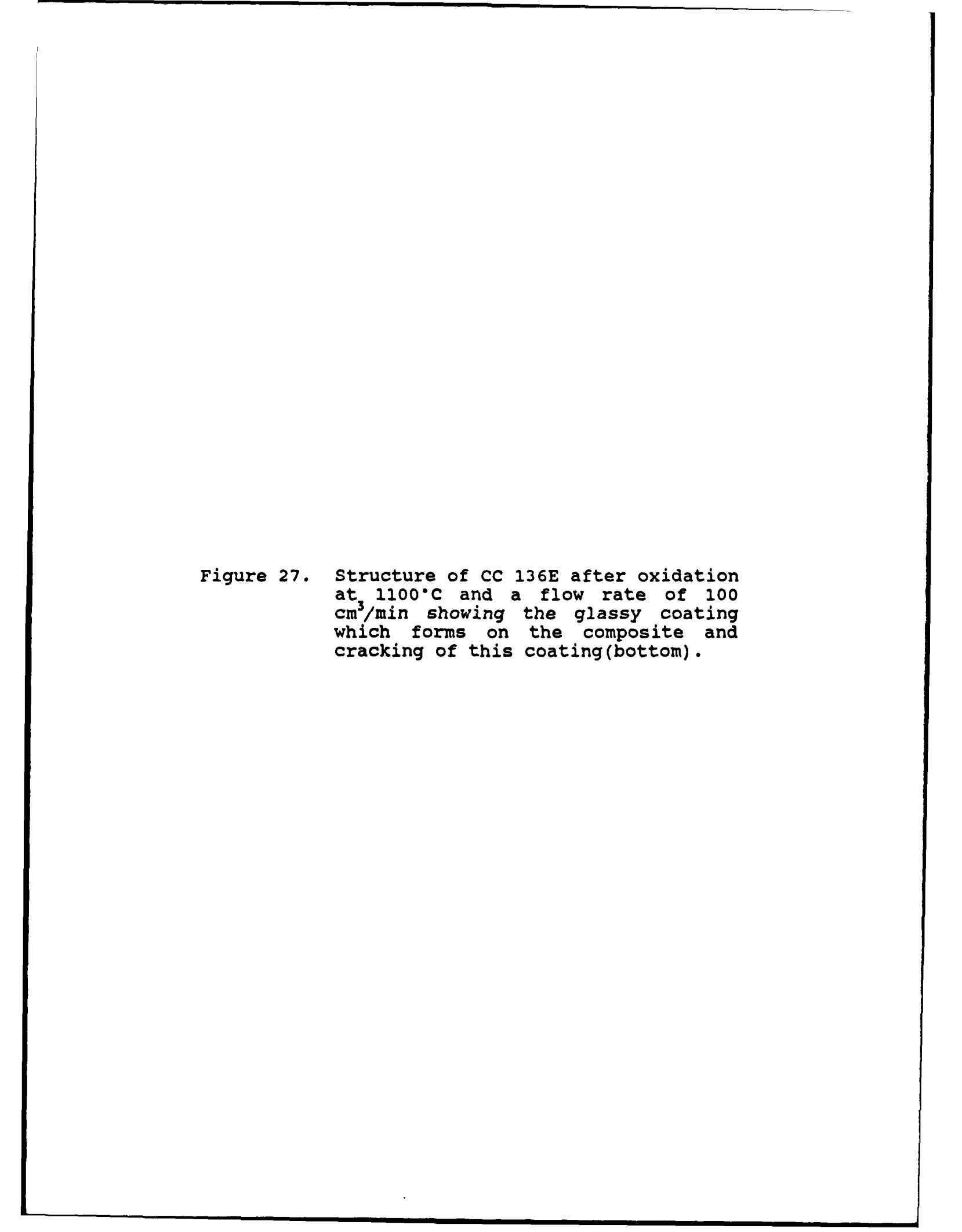

Figure 27. Structure of CC 136E after oxidation at 1100°C and a flow rate of 100 cm^3/min showing the glassy coating which forms on the composite and cracking of this coating(bottom).


2.0KU X50
0330
PITT

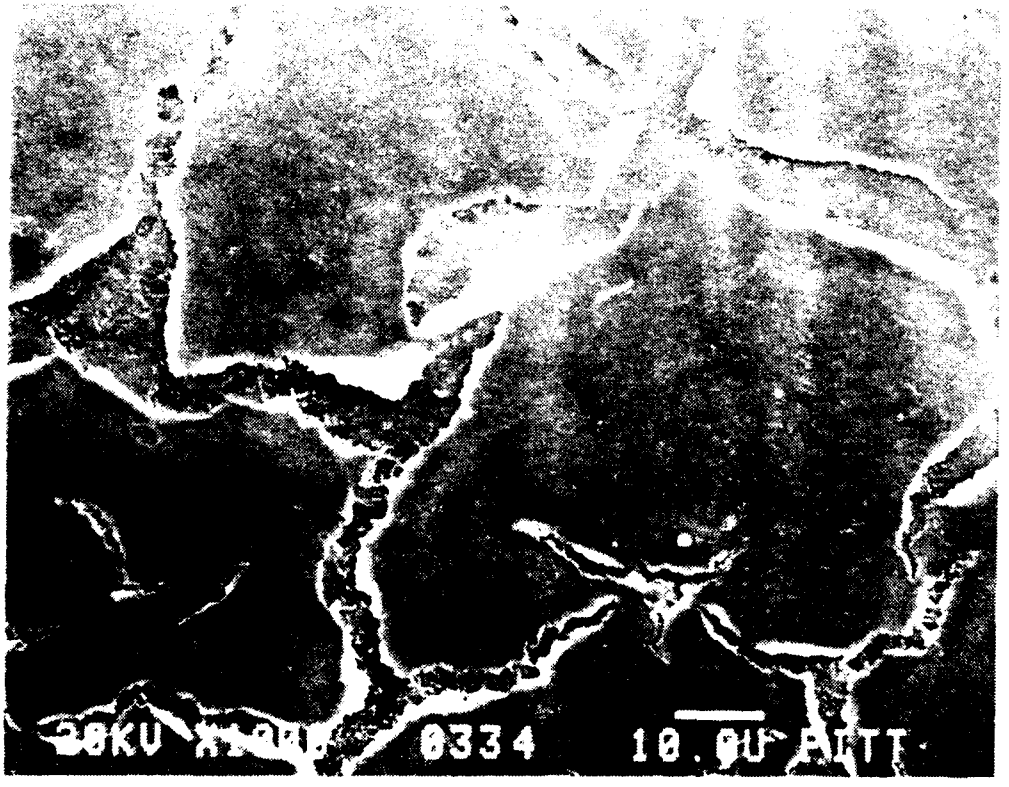
0334
10.0U PITT

Figure 28. Plot of apparent and measured density vs oxidation weight loss for various composites.

DENSITY CHANGES DURING CARBON CARBON OXIDATION

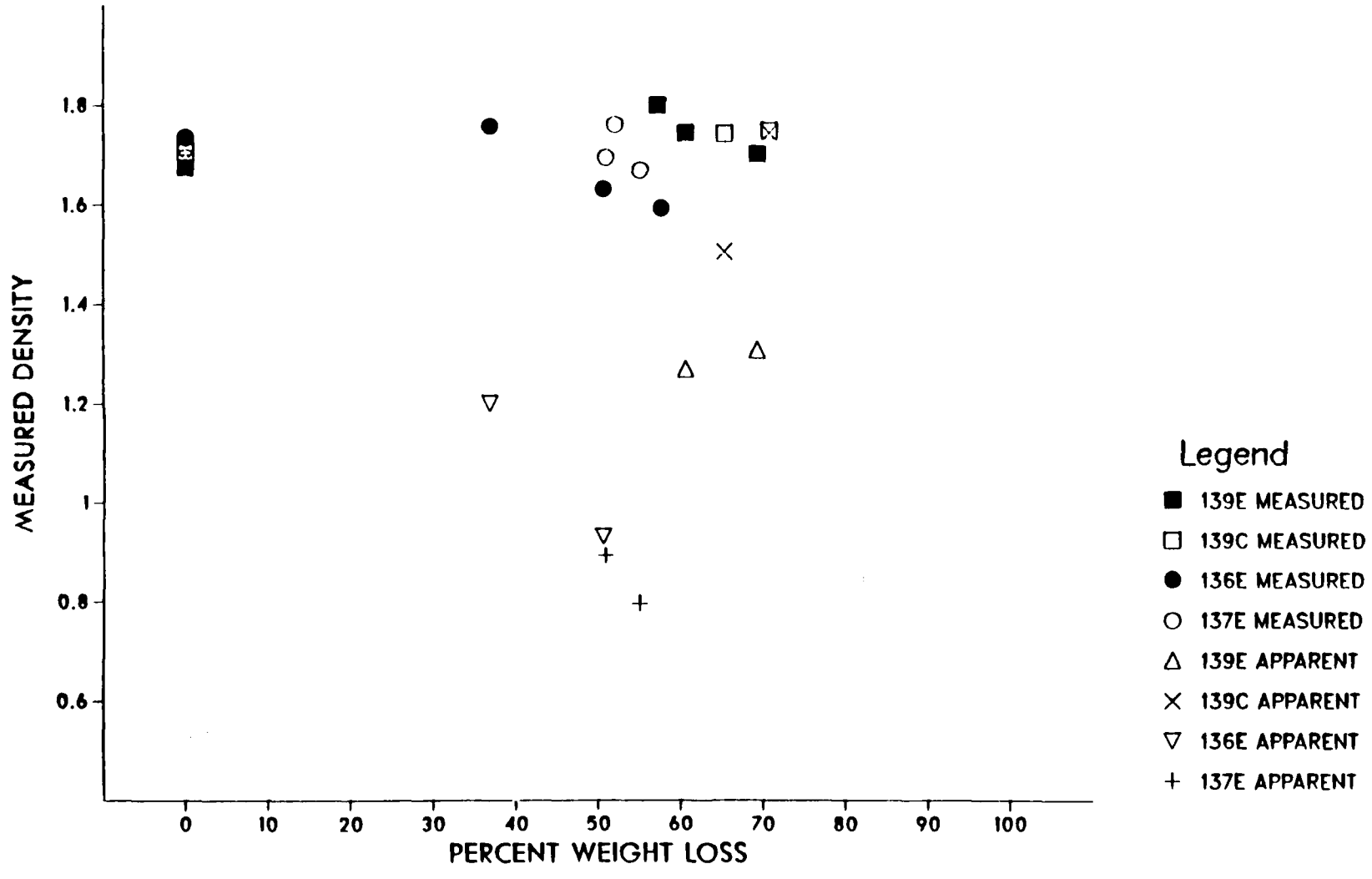

Figure 29. Structure of as-coated HP24 mod/CC 137E. The top micrograph shows the surface structure of the CVD SiC surface. The middle micrograph shows the cross-section of the coating indicating cracks which span the coating thickness. The bottom micrograph shows the coating at higher magnification.

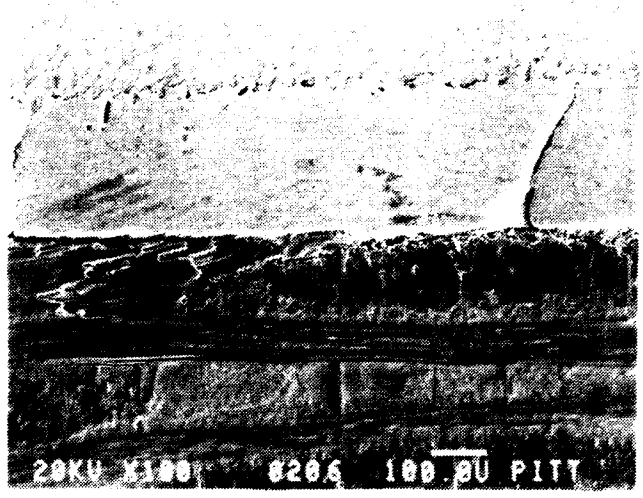
20KV X500 0206 100.0U PITT


SIC
100.0U PITT

Figure 30. Structure of as-processed CC 137E/HP24/M185 which is essentially HP24 mod/CC 137E with an extra glassy coating.

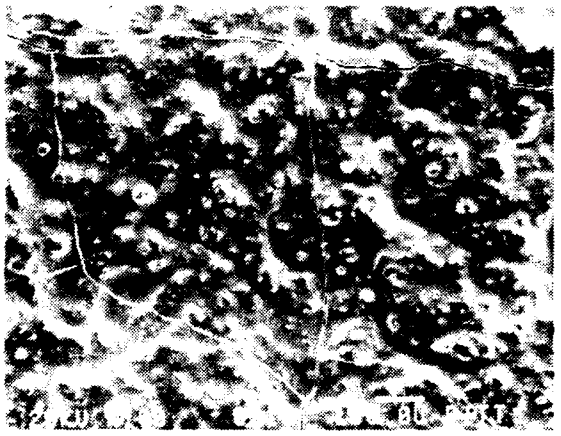

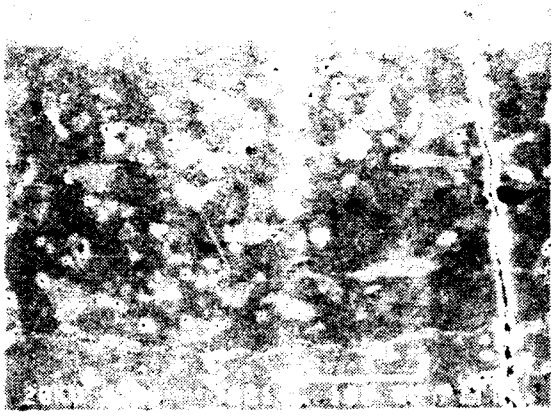

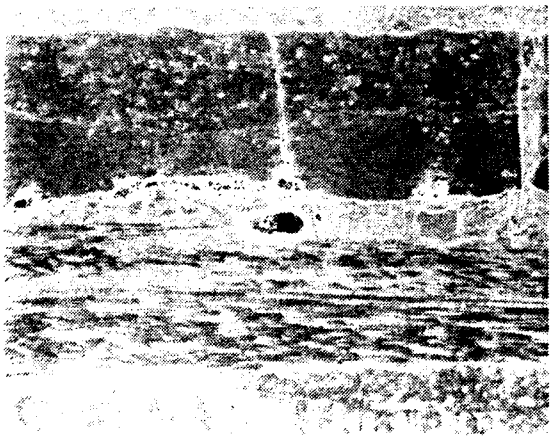

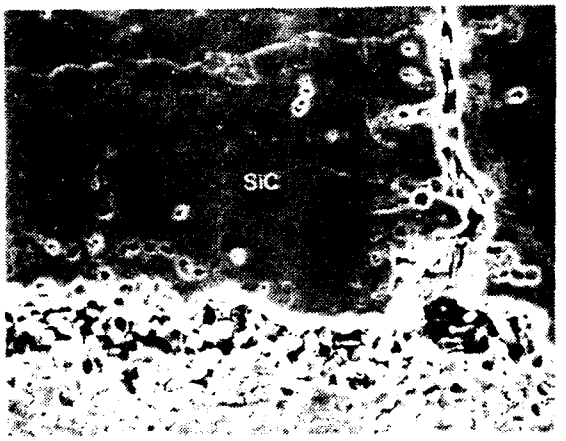
SiC

Figure 31. Structure of as-processed CC 137E/HP24Lt./BXC/RT42A/Glaze which is similar to Fig. 30 except for a much more complex outer glassy coating containing boron and silicon carbides.

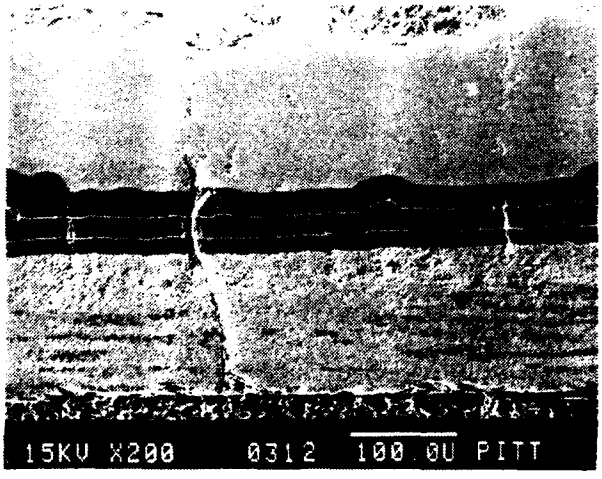
15KV X200 0312 100 0U PITT